npj | acoustics

Review

https://doi.org/10.1038/s44384-025-00024-7

Imaging strategies to assess efficacy and safety of ultrasound-induced blood-brain barrier opening

Check for updates

Gwenaël Pagé[1], Anthony Novell[2] ✉ & Benoît Larrat[1,3]

Focused-ultrasound (FUS) in conjunction with microbubbles contrast agent is a non-invasive methods to induce transient blood brain barrier (BBB) disruption. This review aims to provide an overview of the imaging strategies (magnetic resonance imaging, positron emission tomography, and ultrasound imaging) used in parallel with FUS-induced BBB opening in pre-clinical and clinical studies to ensure the safety and efficacy of the technique.

The blood-brain barrier (BBB) is a semipermeable structure that serves as a critical protective interface between the central nervous system (CNS) and the bloodstream. It is primarily composed of brain endothelial cells that are closely connected by complex tight junctions, creating a highly selective permeability barrier[1]. This selective permeability is crucial for maintaining brain homeostasis and protecting the brain from harmful agents. The BBB regulates drug entry into the brain through transporters that operate via active or passive mechanisms. While these transporters protect the brain from neurotoxic effects, they also limit the effectiveness of drugs intended to target the brain. To overcome this challenge, a technique combining focused ultrasound (FUS) and the administration of intravascular contrast agents, such as clinically approved microbubbles (MBs), has been introduced as a non-invasive method that reversibly and temporarily disrupts the BBB[2,3]. This process allows therapeutic agents, including large molecules such as antibodies[4], nanoparticles[5], and gene therapies[6], to penetrate the brain parenchyma.

Briefly FUS, uses high-frequency acoustic waves to precisely target specific regions of the brain. When exposed to FUS, MBs oscillate within brain capillaries in a process called cavitation, exerting mechanical forces on endothelial cells. Depending on the acoustic pressure, MBs can undergo either stable or inertial cavitation. During stable cavitation, MBs undergo low-amplitude volumetric oscillations at low acoustic pressures, increasing the permeability of the BBB without causing vascular damage[7,8]. This temporarily disrupts tight junctions and enhances transcellular transport, with BBB integrity typically restored within hours, minimizing the risk of long-term adverse effects[9]. In contrast, inertial cavitation occurs when MBs expand and collapse violently, which can lead to vascular disruption[10]. Therefore, controlling the ultrasound dose is crucial to safely disrupt the BBB without causing damage, though skull heterogeneities complicate dose control. Additionally, since MB size and concentration vary over time, it is important to adjust the acoustic pressure during the procedure to avoid the transition to inertial cavitation.

While FUS-mediated BBB opening offers a novel method for delivering therapeutics to the CNS, it introduces several new safety considerations. These include the need for accurate targeting, the risk of tissue heating, the necessity for real time monitoring of microbubble cavitation in situ, and ensuring that the mechanical forces generated are sufficient to disrupt the BBB without causing irreversible vascular or neuronal damage[11,12]. Evaluating the long-term effects of repeated BBB opening on brain function and pathology is also necessary to ensure sustained therapeutic benefits and safety[13]. In addition to safety assessment, the efficacy of FUS-mediated BBB opening needs to be evaluated by guaranteeing that the BBB opening is sufficient to permit drug delivery without compromising barrier integrity[9,14]. Moreover, therapeutic outcomes should be considered as part of the technique's efficacy by demonstrating that FUS-mediated BBB opening improves the delivery and effectiveness of therapeutic agents in preclinical and clinical studies, which is essential for validating this approach[15].

In the last two decades, multiple imaging methods such as magnetic resonance imaging (MRI), nuclear imaging (single photon emission computed tomography (SPECT), positron emission tomography (PET)), and ultrasound (US) have emerged to non-invasively assess the safety and efficacy of FUS-mediated BBB opening. Although neuronavigation-guided FUS has been developed as an alternative to FUS guided with MRI for providing accurate targeting, MRI sequences are still extensively used to ensure the safety and efficacy of FUS-mediated BBB opening. Standard magnetic resonance (MR) sequences combined with MR contrast agents can be used to assess and quantify BBB opening or reclosure[9,16], while specific MR sequences are capable of imaging brain integrity[11,17]. While nuclear imaging and US are less commonly used than MRI for evaluating BBB opening, the ability of PET to investigate neuroinflammation or drug delivery, along with the high temporal resolution and real-time monitoring capabilities of US, makes these modalities valuable tools for assessing the effects of the FUS therapy or for the control of the FUS protocol[18].

[1]Université Paris-Saclay, CEA, CNRS, Baobab, NeuroSpin, Gif-sur-Yvette, France. [2]Université Paris-Saclay, CEA, CNRS, Inserm, BioMaps, SHFJ, Orsay, France. [3]TheraSonic, Paris, France. ✉e-mail: Anthony.novell@universite-paris-saclay.fr

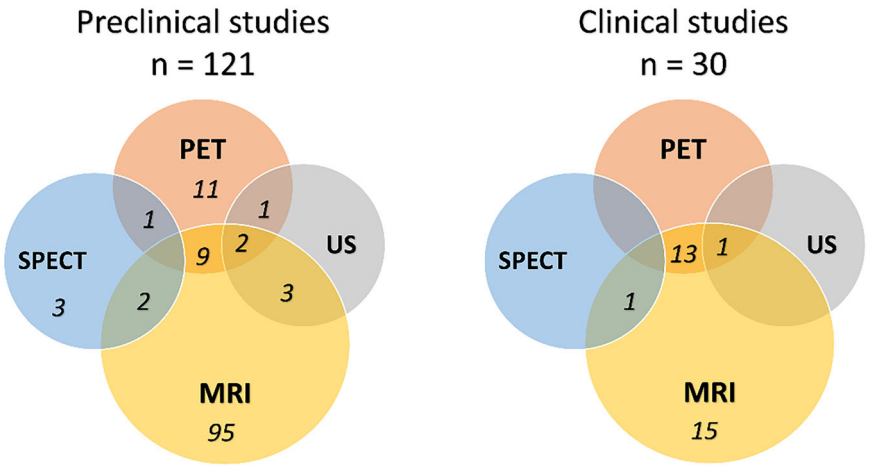

Fig. 1 | Repartition of preclinical studies and clinical studies using MRI, PET, SPECT, and US to assess the safety and efficacy of FUS-induced BBB opening procedure.

This review aims to present the different imaging modalities and non-invasive methods currently used in preclinical and clinical studies to assess FUS-mediated BBB opening.

Methodology

A search began on PubMed in May 2024 with the following keywords: ("blood-brain barrier opening" OR ("BBB")) AND ("focused ultrasound" OR ("FUS")) AND ("magnetic resonance imaging" OR ("MRI") OR (positron emission tomography") OR ("PET") OR ("SPECT") OR ("single photon emission computed tomography") OR ("ultrasound imaging") OR ("US"). After screening the results, we found 151 eligible studies: 121 preclinical studies and 30 clinical studies (Fig. 1). It can be noted that among the 30 clinical studies, one study included mice[19] and non-human primate (NHP)[20] in addition to Alzheimer's patients. In preclinical or clinical studies, MRI is the main imaging modality used to investigate BBB opening. MRI is present in 90% of the publications assessed here for preclinical studies. Moreover, for clinical investigations, every study included an MRI protocol for safety or efficacy assessment. This can be explained by the fact that MRI is the most suitable imaging modality to describe the anatomy and the functionality of the human brain. In contrast, the application of ultrasound imaging is more challenging due to the skull, which attenuates and induces aberrations in the ultrasound waves. Additionally, PET imaging requires specific radiotracers to investigate BBB closure dynamics or neuroinflammation, which are not readily available in all research centers.

Among the 30 clinical studies, 14 combined MRI and PET imaging, and one study associated ultrasound imaging and PET with MRI. PET imaging was used alone in BBB opening assessments for 11 preclinical studies, while ultrasound imaging was always combined with another imaging modality, either with MRI ($n = 3$) or PET ($n = 1$). Finally, two preclinical studies used all three imaging modalities to investigate BBB opening safety and efficacy.

Imaging methods to assess the efficacy of FUS-induced BBB opening

Although PET imaging has recently proven effective for investigating the efficacy of FUS-induced BBB opening, MRI remains the primary modality used for this application, particularly for assessing the dynamics of FUS-mediated BBB opening and closure. However, PET excels in evaluating drug efficacy, where it is a more suitable imaging technique compared to MRI and ultrasound. Techniques for assessing the dynamics of BBB opening and closure, as well as investigating drug delivery, are described in the following sections.

Dynamics of FUS-induced BBB opening and closure

Few MR sequences are used to investigate BBB opening and closure (Table 1). Additionally, T1-weighted imaging (T1w) with contrast agent injection is the technique most commonly applied. T1w imaging can be further categorized into two types of sequences: T1-weighted contrast-enhanced (CE) and T1-weighted dynamic contrast-enhanced (DCE).

T1w Contrast-enhanced. Among the studies focused on FUS-induced BBB opening, MRI is used to assess efficacy in almost all cases, with only three studies not evaluating efficacy. Additionally, 81 studies (79%) used T1-weighted contrast-enhanced (T1w-CE) imaging to investigate FUS + MB efficacy, while T1-weighted dynamic contrast-enhanced (T1w-DCE) imaging was used in 21 studies (20%).

The principle of T1w-CE involves administering a gadolinium-based contrast agent, which shortens the T1 relaxation time and increases signal intensity on T1-weighted images, making areas with disrupted BBB appear hyperintense. Commercial MR contrast agents typically range in size from 1 to 60 nm[9], which is small enough to cross the BBB and diffuse within the brain, as FUS-induced BBB permeabilization facilitates the passage of particles smaller than 65 nm from the bloodstream to the brain[9,14].

Most publications using T1w-CE focused on obtaining qualitative information and observing signal enhancement at the focal point of the ultrasound[21], as shown in Fig. 2. However, some studies used T1w-CE images to quantify the volume of BBB opening. To quantify the BBB opening volume at the sonicated site, an intensity threshold was determined, and contrast-enhanced pixels in the vessels and ventricles were excluded[22,23]. Mean MR signal intensity enhancement was also plotted as a function of burst length, pulse repetition, and contrast agent dosage[16]. This analysis indicated that the magnitude of BBB disruption induced by ultrasound pulses does not depend on pulse repetition frequency or dosage of the ultrasound contrast agent, but decreases as burst length is shortened. Several studies have demonstrated a relationship between BBB opening volume and signal enhancement from T1w-CE images with the acoustic parameters used during sonication[24,25].

For visualization, classic T1w sequences such as Multi-Slice Multi-Echo[21], SNAP gradient echo[26], fast spin echo[16], or rapid acquisition refocused echoes[27] can be used. More sophisticated sequences, such as T1 mapping, can provide quantitative information. These studies use quantitative contrast agent concentration maps to evaluate BBB disruption, relying on parametric T1 maps rather than T1w-CE images[9,28,29]. Specifically, Fast Gradient Echo images acquired at different time points after magnetization inversion are used to sample the T1 recovery curve. This approach allows for determining the time window for delivering an agent of a given molecular size[9]. A The same group provided a full mathematical model of this approach in 2019[30].

Using T1 mapping, Marty et al. observed the dynamics of FUS-mediated BBB opening. Their study found that contrast agent concentration persisted even 24 hours after BBB opening[9]. To assess the efficacy of FUS-induced BBB opening and its reversibility, T1w-CE sequences should be applied at multiple time points. For T1 mapping, a pre-contrast enhancement acquisition before the sonication procedure is required for

Table 1 | MR sequences applied to assess BBB opening and closure

Sequence	1.5 T	3 T	4.7 T	7 T	9.4 T	11.7 T
T1w-CE	14,16,31,86,104,156–158	13,20,22,32,33,38,40,43,50–52,69,84,94,99,107,114,159–166	41,66,167	9,12,21,27–29,34,37,56,70,74,83,93,108,113,168–177	19,23,24,26,35,39,44,45,54,71,101,109,155,178–185	96
T1w-DCE		11,17,50,52		42,53,57,87,186–188	25,35,39,45–47,189–192	
T2w					44,54	
DTI		38				

T1w-CE T1-weighted contrast-enhanced, *T1w-DCE* T1-weighted dynamic contrast-enhanced, *T2w* T2-weighted, *DTI* diffusion tensor imaging.

quantitative analysis[9,29]. In contrast, with "classic" T1w-CE sequences, a pre-contrast-enhancement acquisition is not necessary, although some studies still perform T1w-CE before FUS + MB procedures[31–36] for estimating the volume of BBB opening. T1w-CE is typically acquired immediately after the sonication procedure. In preclinical studies, MR-guided FUS systems are advantageous as they allow T1w-CE sequence acquisition just a few minutes after BBB + FUS procedures[37]. In these setups, the MR contrast agent is injected before sonication, just after MBs. Studies usually report acquiring T1w-CE images at 15 minutes[23,31], 30 min[27,38,39], or up to 1 hour[40], depending on factors such as positioning the animal inside the MR scanner after FUS + MB procedures or the number of scans needed before contrast agent injection[41]. To confirm BBB closure, most studies perform a T1w-CE scan 24 hours after sonication[20,28,35,42], although it is less common to acquire the sequence 72 hours after FUS + MB procedures[32,39]. T1w-CE sequences are typically acquired shortly after contrast agent injection, ranging from 2 minutes to 2 hours[22,43–46], and the choice of contrast agent can also influence the quality of BBB opening assessment after FUS + MB procedures[28].

T1w Dynamic contrast-enhanced. The second most commonly applied MR sequence for investigating BBB opening is T1w-DCE[17,47]. This sequence quantitatively evaluates the time evolution of local BBB permeability induced by FUS applications. T1w-DCE imaging requires acquisitions both before and after contrast injection to generate a time-intensity curve[48]. The timing of these acquisitions relative to the sonication procedure is similar to that used for T1w-CE scanning[42,45].

The T1w-DCE sequence involves acquiring a series of images to create the time-intensity curve. Studies have reported acquiring up to 40 volumes of images with a temporal resolution of 3.5–6 seconds. To calculate the K_{trans} parameters, which represents the pharmacokinetics of the MR tracer through the opened BBB, the general kinetic model[49] is most widely employed[47,50,51]. Permeability maps generated with the T1w-DCE sequence have been used to assess the impact of microbubbles or acoustic pressure on permeability maps[52,53], the dependence of acoustic parameters on closure rate[23], and the influence of neurological disease on closure rate[35].

Other MR sequences. Some studies have reported using T2-weighted (T2w) or DTI sequences to assess BBB opening following FUS + MB procedures, instead of relying solely on T1w imaging[38,44,54]. In 2005 and 2007, Choi and colleagues utilized a T2w sequence to evaluate BBB opening with gadolinium injection 15 minutes after sonication[44,54]. However, most of the critical information was derived from T1w-CE images acquired during the same session as the T2w images.

In 2021, Karakatsani et al. conducted diffusion tensor imaging (DTI) with spin echo planar imaging before the injection of gadodiamide[38]. They observed that DTI without contrast produced similar results to those obtained from T1w-CE after contrast agent injection, highlighting the potential of DTI sequences to assess BBB opening following FUS + MB procedures.

Positron emission tomography. Compared to MRI, PET is a sensitive and quantitative molecular imaging technique that can measure tracer distribution, uptake, and the pharmacokinetics of drug delivery within the brain. PET scans not only assess tissue activity but also quantify the actual amount of radiopharmaceuticals delivered to the tissue during the scan. Moreover, PET is highly sensitive in detecting changes in regional cerebral metabolism and identifying specific neuroimaging patterns. Thus, PET is particularly suitable for monitoring the transport of radiotracers across the BBB[15].

Several radiotracers have been employed to investigate BBB integrity following BBB + MB procedures (Table 2). In an initial study, Yang et al.[55], demonstrated the utility of PET in assessing the degree of BBB disruption induced by ultrasound (US), by injecting a dose of 22.2 MBq of [18 F]-FBPA immediately after sonication. Later, Okada et al.[56] and Liu et al.[57] found that [3-11 C] isobutyric acid and [68Ga]-bevacizumab, respectively, showed significant accumulation in the sonicated area compared to the non-

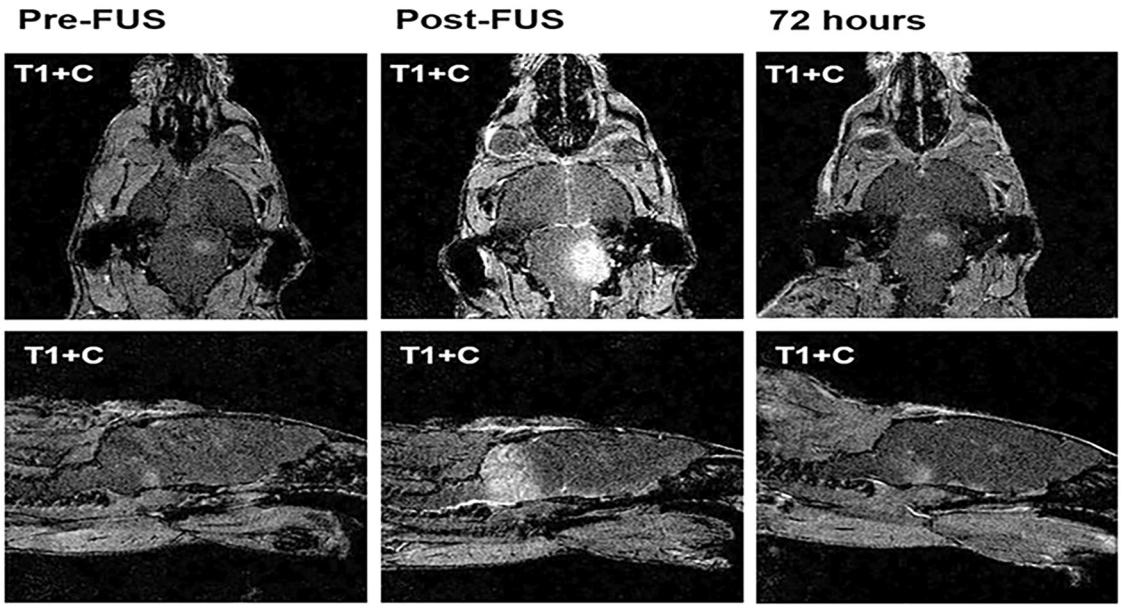

Fig. 2 | T1w-CE MR imaging showing sonication of tumor and peritumoral region. BBB closure demonstrated at 72 hours after FUS. Figure adapted with permission from ref. 155.

sonicated area. A notable advantage of [3-11 C] isobutyric acid is its unidirectional transport from the blood to the brain and its favorable kinetic properties for assessing BBB opening.

More recently, several other radiotracers have been utilized to investigate BBB disruption. Hugon et al. proposed the use of [18 F]2-fluoro-2-deoxy-sorbitol (FDS)[58,59], administered intravenously at a dose of 4.2 MBq, with dynamic PET acquisition lasting 60 minutes immediately after sonication, Fig. 3. This radiotracer provided a sensitive imaging marker to dynamically measure BBB permeability variations over a timescale of minutes. Additionally, the injection of 4.7–5.7 MBq of [18F]-FSPG[60] and of 20 MBq [99mTc]Tc-DTPA[61], followed by 30 min of PET acquisition, was suggested to assess BBB permeability. Similar to MRI, PET imaging is typically conducted immediately after sonication to evaluate BBB permeability. Follow-up acquisitions may be performed three hours[61] after FUS + MB procedures to assess the dynamics of BBB opening, with another acquisition 24 h post-sonication to evaluate the reversibility of the procedure[59,61,62].

The potential of nanoclusters in assessing BBB opening has been explored in a series of three publications[63–65]. PET imaging with [64Cu]-AuNCs confirmed effective penetration, retention, and diffusion in the brain post FUS + MB treatment. However, the application of these nanoclusters in clinical studies is limited due to their high cost, poor therapeutic efficacy, and challenges in degradation, which complicates their repeated use as a therapeutic modality[66].

Role of efflux pump. If FUS-mediated BBB opening can disrupt the physical barrier, another obstacle remains that hinders effective drug delivery to the brain: efflux transporters, such as P-glycoprotein (P-gp), which serve as a functional barrier to prevent harmful compounds from entering the brain[67]. Therefore, the physical and functional aspects of the BBB complement each other in limiting the ability of most drugs to reach the brain parenchyma and exert effects on the CNS[68]. Studies have reported varying results regarding the impact of FUS on the expression and functionality of P-gp[34,69–72].

Using PET imaging with radiolabeled substrates of ABC transporters to study efflux transporter function at the BBB[73], Goutal and colleagues[74] applied PET imaging with [11C]-erlotinib immediately after sonication and observed no increase in brain uptake of [11C]-erlotinib. However, when an inhibitor (elacridar) was applied, the uptake of radiotracers increased, and erlotinib was delivered to the brain with or without FUS application, suggesting that FUS affects only BBB integrity, not its functional role. These findings were confirmed by the same group in 2023[21], where they injected a bolus of 38.2 ± 5.7 MBq of [11C]-metoclopramide 10 minutes after sonication, followed by 30 minutes of dynamic PET scans. In this study, they found no effect of FUS-mediated BBB opening on the brain kinetics of [11C]-metoclopramide, suggesting that nearly complete down-regulation of P-gp expression is required to enhance brain delivery of compounds limited by P-gp-mediated efflux, rather than just altering BBB integrity.

Passive acoustic mapping. As described in section 4, US with passive cavitation imaging provides information on the cavitation regime to ensure the safety of the procedure. A key advantage of US imaging is that passive acoustic mapping (PAM) not only offers safety information but also detects and localizes cavitation activity during the FUS procedure. However, this technique is limited by low spatial resolution, especially when using a linear array transducer, due to the small receiving aperture and uncertainty regarding the timing of cavitation events. Additionally, the point spread function of passive acoustic mapping is compromised, as only low-frequency acoustic signals can be detected through the skull, and the signal is further distorted by its propagation through inhomogeneous tissue and skull bone[75], Fig. 4.

Several methods have been proposed to map cavitation activity. An early approach developed a time-exposure acoustics method using an array transducer to map cavitation activity from passively acquired ultrasonic data[76]. In this method, a standard diagnostic array is placed coaxially with the FUS transducer, and signals received passively by 64 elements are combined using time-exposure acoustics to generate maps of inertially cavitating regions during the FUS procedure. While this technique produced cavitation maps consistent with simulation and theory, it was only applied in agar gel, which differs from the heterogeneous medium encountered in preclinical and clinical settings. Additionally, two sparse deconvolution algorithms were used to deconvolve inertial cavitation emissions based on the assumption of temporal sparsity of cavitation emissions, but balancing improvements in resolution (5 mm axial resolution) with robustness proved challenging. Subsequent studies developed improved methods for enhancing spatial resolution and robustness to noise in cavitation mapping, utilizing robust Capon beamformer and eigenspace-based robust Capon beamformer techniques[77]. However, these studies employed high-frequency harmonic signals (>5 MHz), which are not suitable for transcranial imaging.

In 2018, Wu and colleagues conducted FUS treatments in non-human primates (NHPs) during a brief procedure (30 min) without the need for

Table 2 | MR imaging sequences used to investigate BBB opening safety in preclinical studies

Sequence	1.5 T	3 T	4.7 T	7 T	9.4 T	11.7 T	Assessment
T2w	14,31,86,104,157	11,13,17,20,22,32,40,43,50–52,84,99,161–163,165,166,186	51	9,28,37,42,70,74,83,108,168,171,173	19,45,47,71,109,178,180		Edema
T2*w	31	20,69,94,99,107,159–161,163,164,166		69,74,108,168,171	83	96	Micro-hemorrage
SWI		11,13,17,20,22,32,40,43,50,51,84,186		42,53			Micro-hemorrage
Thermometry	14,86	35					Temperature
DWI	31	20,38		29			Ischemic necrosis
T1w-CE					24		BBB opening location
ARFI				9,28,37,70,93			FUS location
CEST					109		Metabolic imaging
BOLD		114		12,36,113,169			Neural activity
ASL			41	12,29			Blood perfusion
DTI			41		109		Fiber structure
MRE				168			Tissue mechanical properties
MRA		84					Vessel anatomy

T2w T2-weighted, *SWI* Susceptibility weighted imaging, *DWI* Diffusion weighted imaging, *T1w-CE* T1-weighted contrast-enhanced, *ARFI* acoustic radiation force impulse, *CEST* chemical exchange saturation transfer, *BOLD* Blood oxygenation level-dependent, *ASL* arterial spin labeling, *DTI* diffusion tensor imaging, *MRE* magnetic resonance elastography, *MRA* magnetic resonance angiography.

online MR guidance, using real-time targeting and acoustic mapping to assess the effectiveness and safety of the procedure[40]. They developed a time-exposure acoustics technique, combined with parallel beamforming, which reconstructed passive acoustic maps in real-time during the FUS + MB procedure by multiplying a reconstruction sparse matrix with the radio-frequency channel data. However, only a small portion of the received data (a few microseconds out of 10 ms) was processed. To accelerate computation, sparse matrix multiplication was proposed[78]. potentially expanding the field of view (FOV) and enabling real-time detection of off-target cavitation activity. Nevertheless, the improvement was insufficient for real-time PAM with the full temporal integration of the 10 ms burst, and it was shown that acquiring the full burst acoustic emission signal during sonication is critical[79].

Later, Bae and colleagues[75] developed a real-time cavitation mapping technique capable of providing full-burst analysis using a parallel processing scheme based on coherence-factor PAM to enhance spatial resolution. The cavitation map was spatially correlated with the BBB opening region, as confirmed by contrast-enhanced MRI, demonstrating efficacy in NHPs for providing real-time cavitation monitoring to ensure safe and effective BBB disruption. However, further improvements are needed, such as utilizing a matrix array transducer that can produce 3D volumes of cavitation activity to detect out-of-plane acoustic emissions.

Finally, a recent ultrasound imaging study demonstrated the potential of ultrasound to assess BBB integrity following FUS-induced BBB opening. In 2022, Singh et al. combined power cavitation mapping with PAM to precisely target FUS in rodents[66]. This study showcased an ultrasound-based approach for ensuring the efficacy of focused ultrasound with high precision in small animals.

Monitor drug delivery after BBB disruption

Another approach to assess the efficacy of BBB disruption is by monitoring drug delivery following FUS + MB procedures. PET imaging offers significant advantages over other modalities in this context, as it enables detailed analysis of pharmacokinetics, including absorption, distribution, metabolism, and excretion of drugs. To evaluate whether drugs can cross the BBB after FUS + MB procedures, it is necessary to radiolabel the molecule. Radiotracers used in PET imaging have different half-lifes, such as [11C] (20 minutes), [18F] (109.8 minutes), or [89Zr] (78.4 hours). Thus, investigation of drug delivery depends on the radiotracer. By using [89Zr] with a long half-life, it is then possible to explore the deposition of antibodies characterized by a long plasma lifetime. For example, topotecan, a chemotherapeutic agent used for ovarian and lung cancer, has been radiolabeled with [11C]. A dose of 5.4–7.9 MBq of [11C]-topotecan was injected into mice, followed by a 60-minute dynamic PET acquisition[60]. Kinetic analysis of [11C]-topotecan brain uptake demonstrated the potential of this radiotracer to predict the locoregional brain concentration of topotecan in patients. Other studies have shown the ability of PET to quantify the accumulation of adenovirus [64Cu]-AAV9[80], or antibodies 89Zr-DFO-C4, 89Zr-DFO-C4Fc-MUT[59], or [89Zr]-Cetuximab(CTX)[19,81] after BBB disruption in mice with glioblastoma. Interestingly, in the case of the [89Zr]-CTX, if for one study, FUS-mediated BBB opening did not enhance the long-term accumulation and retention of antibody in orthotopic glioblastoma compared to a control group without FUS[19]. A second study shows the use of [89Zr]-labeled CTX with an increase in the uptake of [89Zr]-DFO-CTX in the sonicated brain area (two times compared to the intact BBB brain mice group), and it was possible to evaluate CTX until one week[81].

Regarding the timing of PET acquisitions, they are typically performed immediately after sonication. Most studies report that imaging was conducted 10 to 30 minutes after FUS-mediated BBB opening procedures[59,60,80]. Some studies also evaluated drug uptake at multiple time points, ranging from radiotracer injection to 7 days post-procedure[59,82]. Additionally, a study highlighted the importance of timing between [89Zr]-mCD47 injection and FUS + MB procedures in mice, demonstrating how repeated sonication can enhance drug delivery[33].

In 2016, Liu and colleagues demonstrated that (68Ga)-bevacizumab uptake was improved after FUS procedures, with results comparable to

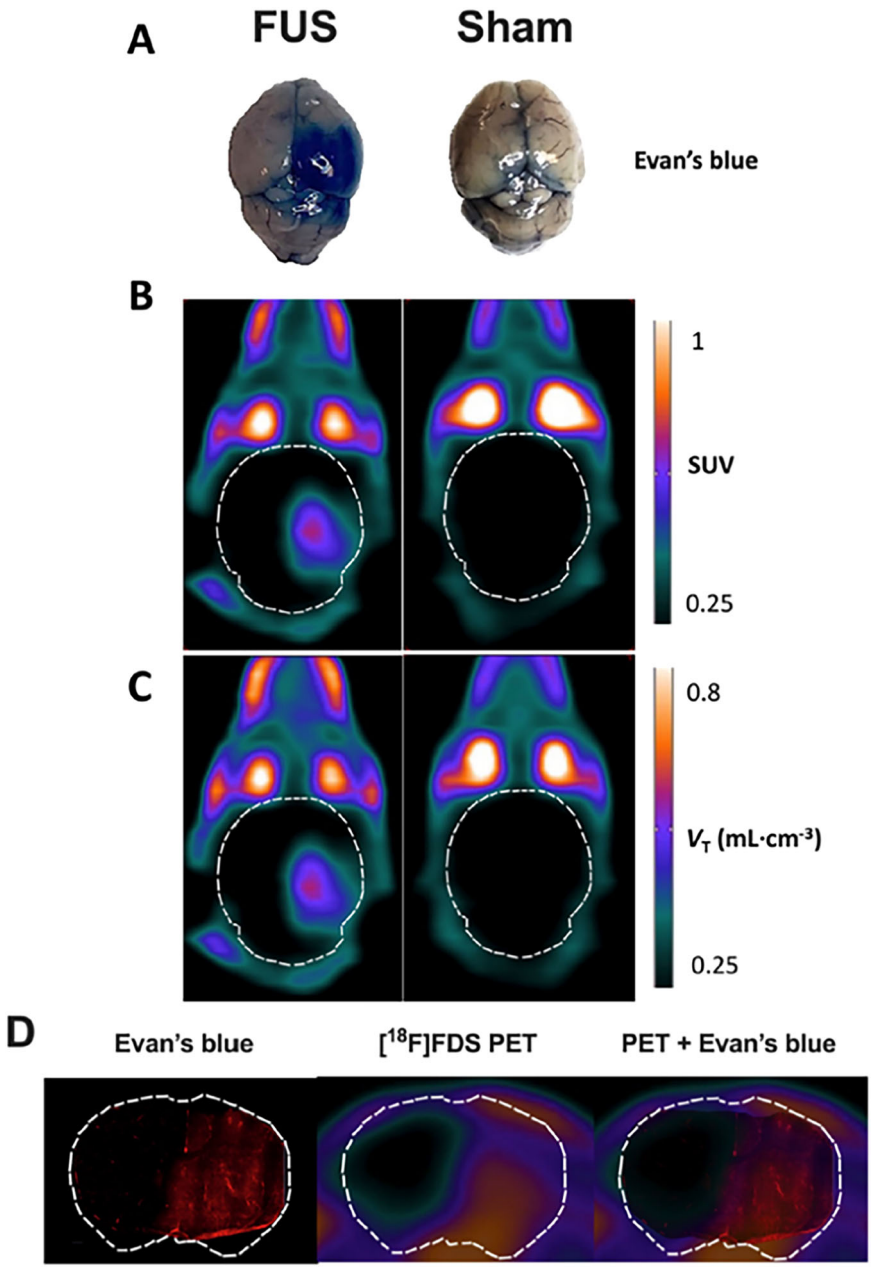

Fig. 3 | Impact of FUS on BBB integrity assessed Impact of focused ultrasound (FUS) on blood–brain barrier (BBB) integrity assessed using Evan's blue extravasation and positron emission tomography (PET) using [18F]2-fluoro-2-deoxy-sorbitol ([18F]-FDS). Extravasation of Evan's blue was obvious in the right brain hemisphere of animals of the FUS group (**A**). Standardized uptake value (SUV)-normalized brain PET images (sum 30–60 min) of [18 F]FDS uptake after hemispheric BBB disruption induced by focused ultrasound (FUS) or without (sham) are shown in **B**. Corresponding parametric images describing the total volume of distribution (VT), estimated using the one-tissue compartment model from 0 to 60 min are shown in (**C**). In (**D**), the distribution of the fluorescence of the Evan's blue dye in a coronal slice of mouse brain after the FUS protocol obtained ex vivo was overlaid to corresponding slice of [18F]-FDS PET image obtained in vivo in the same animal. Figure reproduced with permission from[58].

those obtained with MRI using T1w-DCE acquisition and gadopentetate dimeglumine (Magnevist) injection[57]. Indeed, several models have employed T1w-DCE or T1w-CE mapping to estimate molecular penetration[28,42,83]. One such model was developed to estimate the distribution of molecules of various sizes[42], while another model predicted particle distributions based on MR contrast agent concentration maps, considering ultrasound acoustic parameters, particle size, blood pharmacokinetics, and molecular ADC[28].

In ultrasound, the role of transcranial cavitation monitoring was demonstrated in NHPs, where a correlation was observed between cavitation activity and the amount and concentration of gadolinium delivered through the BBB, as seen in T1w images[84]. A subsequent study highlighted the potential of passive cavitation imaging to predict the location and concentration of nanoclusters delivered through FUS-induced BBB opening[85]. The authors found a correlation between passive cavitation imaging dose mapping and in vivo PET images, demonstrating the potential of this strategy to guide the sonication procedure and achieve conformal delivery of therapeutic agents to the targeted brain region.

Imaging methods used to ensure the safety of FUS-induced BBB opening

Imaging provides standardized and reproducible methods for assessing BBB opening, which is crucial for the validation and comparison of different techniques in clinical trials. High-quality imaging data support regulatory approval processes by providing robust evidence of safety, facilitating the translation of BBB opening techniques from research to clinical practice.

Over the last two decades, imaging modalities have been shown to be relevant for providing a real-time monitoring, assessing physiological impact, detecting adverse events such as neuroinflammation or tissue damage and assessing long-term safety of repeated BBB opening. The first step of the safety evaluation of FUS-induced BBB opening is to provide an accurate targeting of FUS. The development of MR-compatible US systems developed for both preclinical and clinical device, MR-guided FUS devices have been developed for rabbit[86], rodents[37], NHPs[87], and patients[88] and have been able to precisely target and monitor FUS during BBB opening procedure. MR devices offer a large variety of sequences to describe brain anatomy and brain functionality that can be exploited to monitor the safety

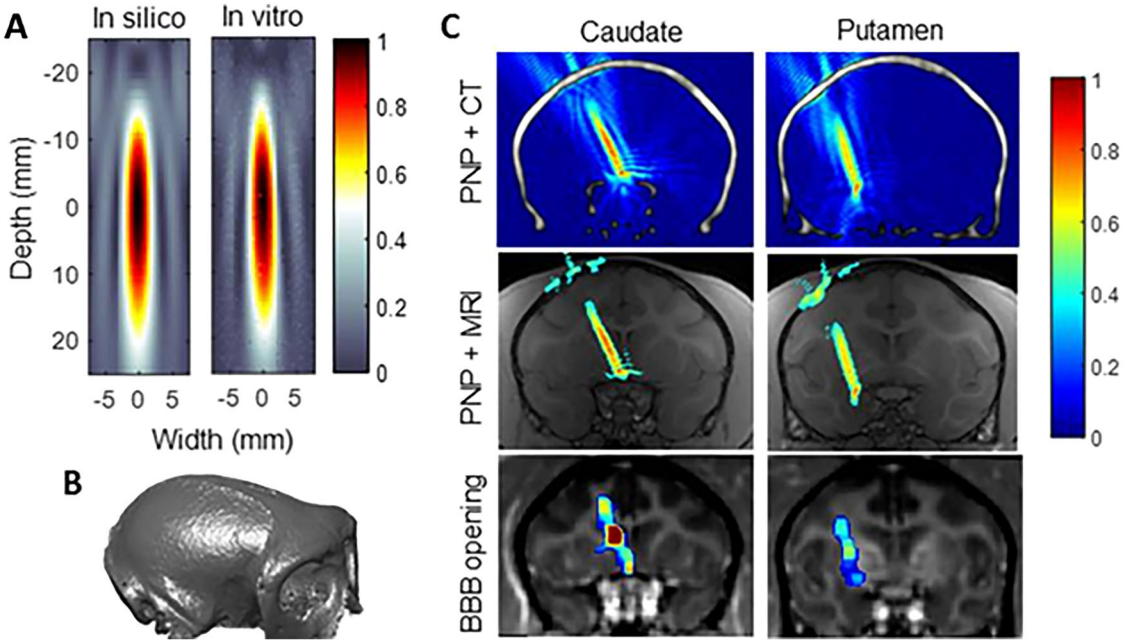

Fig. 4 | Simulation of the acoustic pressure field to estimate the BBB opening. **A** The in silico acoustic profile in the focal region was calibrated to be the same as the profile of the FUS transducer measured in water using a hydrophone. **B** The skull of a monkey from CT used to acquire the acoustic properties of the skull including density and the speed of sound. **C** The simulated transcranial peak-negative pressure (PNP) field (normalized to the pressure without the skull) corresponded to the BBB opening in the caudate and putamen (arbitrary unit, A.U.). Figure adapted with permission from ref. 40.

of sonication procedures (Table 2). Anatomical sequences such as T1w and T2w are essential to precisely targeting FUS procedures, more sophisticated sequence such as acoustic radiation force impulses (ARFI) have also demonstrated their potential[37]. This technique is based on the MR elastography principle, which was initiated in 1995[89,90] and has shown the ability of MRI to reveal submicrometers movements induced by transient shear wave on phase images to estimate tissue mechanical properties. MR-ARFI sequence is able to measure focal tissue displacements caused by FUS in the brain by using a standard spin echo sequence with two additional bipolar sinusoidal gradients equidistant to the 180° radiofrequency pulse and synchronized with the ultrasound burst[91]. The sequence was then optimized for animal and human applications[91,92]. In case of FUS-mediated BBB opening, ARFI acquisition is performed before sonication and injection procedures to localize the FUS spot and to reposition the ultrasound beam in the targeted region of interest[9,28,37,70]. More recently, the MR-ARFI sequence has been improved to target the location of MB-enhanced FUS to monitor cavitation and thus assess BBB integrity without the need of an MR contrast agent[93].

Recently, neuronavigation-guided FUS has shown its ability to guide the focal beam with precision comparable to neurosurgical stereotactic procedures[17], offering significant advantages compared to MR-guided FUS, including lower cost, better accessibility and increasing patient comfort. However, if neuronavigation-guided FUS avoids the need for an MR-compatible US transducer and an MR scanner during sonication, the method is still based on MR images acquired before FUS + MB procedure. Moreover, beyond localization, imaging remains necessary for real-time monitoring during sonication and the evaluation of potential adverse events. The following parts of this section will describe the imaging modalities and sequences used in MRI, PET, or US, highlighting the advantage of each modality[18], to ensure the safety of FUS-mediated BBB opening.

During the FUS-induced BBB opening procedure: To monitor the sonication

As described previously, several developments in preclinical and clinical research have aimed to combine MRI scanners with MR-compatible US transducers[86]. This hybrid system not only allows for guiding FUS using MRI images but also facilitates monitoring the safety of FUS-induced BBB opening procedures through the use of MR thermometry sequences to display tissue heating during sonication[14,86,94]. Apart from the Sonocloud system (Carthera, Lyon, France), where a US device is surgically implanted in the skull bone[95], most of the FUS are applied through the intact skull, and the phenomenon of bone heating can potentially induce brain damage[96]. Thermometry sequences, based on phase mapping, utilize the temperature dependence of the water proton chemical shift to measure temperature changes with an accuracy of ±0.5°C[97]. In preclinical studies involving mice, rabbits, and pigs, thermometry sequences were applied after craniotomy using a gradient echo sequence during sonication[14,86,94]. MR thermometry images have shown temperature elevations and a correlation between tissue heating and histologically measured lesions[86]. Temperature feedback from MR thermometry allows for adjustment of the power level to account for variability in skull shape, density, and tissue perfusion rates. Additionally, a quantitative MR-ARFI-based method has been proposed to measure tissue viscoelastic properties, revealing that elasticity and viscosity decrease while temperature measures from thermometry decrease during FUS applications[98].

Compared to MRI, US imaging offers several technical advantages for monitoring sonication procedures[18]. Ultrasound provides real-time imaging capabilities, enabling immediate assessment and adjustment during BBB opening procedures. This is particularly useful for ensuring precise targeting and monitoring MB cavitation as it occurs. However, the use of ultrasound imaging is limited by the skull, which induces aberrations in the ultrasound waves. Despite this limitation, the interest in passive cavitation mapping has been demonstrated for transcranially mapping microbubble activity in the brain[99]. The passive cavitation imaging technique employs a FUS transducer as a source and an array of receivers to passively record and reconstruct the acoustic field[100]. This method leverages the formation of diverging pressure waves at frequencies different from the FUS device (e.g., harmonics) due to oscillating bubbles. By recording these waves with multiple acoustic receivers, their sources can be back-propagated to reconstruct two- or three-dimensional maps of cavitation activity. The image amplitude indicates the intensity of acoustic emissions, while the spectral content reflects the type of microbubble oscillations and the cavitation regime. This ensures that cavitation occurs at the targeted location and at the desired focal intensity.

The images capture activity at high temporal resolution and can be obtained at a frame rate that allows real-time control of MB-enhanced FUS procedures in the brain. However, passive cavitation mapping has limited spatial resolution, and the technique has been improved with power cavitation mapping, which displays the mean intensity of acoustic cavitation over time and correlates with areas of acoustic cavitation-induced BBB opening. Power cavitation-guided BBB opening with FUS could potentially serve as a standalone system that may not require MRI guidance during the procedure[101].

After the FUS-induced BBB opening procedure: To evaluate potential adverse events

The importance of imaging modalities in assessing the safety of FUS-mediated BBB opening is especially pronounced after the sonication procedure. Imaging data can assist in optimizing the parameters of BBB opening procedures, such as US frequency, acoustic pressure, and microbubble concentration. This optimization enhances therapeutic delivery while minimizing risks. Given the variety of MR sequences available for investigating brain functionality or damage and the ability of PET imaging to assess neuroinflammation, both imaging modalities are commonly used to evaluate potential adverse events. However, only 61% of the MR studies assessed the safety of FUS-induced BBB opening procedures. In cases where acoustic parameters have already been deemed safe, additional safety evaluations may not be necessary.

Vascular assessment

T2w, T2*w and SWI. MRI is the modality typically used to assess vascular damage, such as edema or hemorrhage, which may occur when the BBB is disrupted[102]. Among the various sequences available, T2w imaging is the most commonly used to ensure the safety of BBB opening and detect edema (Table 2). T2w imaging is employed in 39% ($n = 42$) of the preclinical studies utilizing MRI. This sequence needs to be carefully positioned within the MR protocol. MR contrast agents (used to assess BBB opening, see section 3) alter the T2 signal by causing localized inhomogeneities in the magnetic field[103]. Therefore, T2w images are usually acquired before the injection of the contrast agent when the sequence is applied directly after sonication; otherwise, T2w images are acquired one day or a day after injection of the contrast agent. This MR sequence is widely available in both preclinical and clinical scanners and has been successfully applied to detect brain tissue damage in small animals such as mice and rats[9,104] and in large animals such as swine and NHP[17,31].

Immediately following T2w acquisition, T2*w and susceptibility weighted imaging (SWI) are the most common MR sequences used to investigate brain tissue vascular damage, applied in 19 and 14 studies. T2*w is a gradient recalled-echo sequence, without a refocusing 180° radiofrequency pulse, thus making it sensitive to the susceptibility effect[105], while SWI maximizes the susceptibility effect by combining a long echo time, fully flow-compensated 3D gradient echo, and using both the magnitude and filtered phase information[106]. Both techniques are used to detect cerebral microbleeding and, like T2w imaging, must be acquired before contrast agent injection.

In 2008, Liu and colleagues used SWI to detect tissue hemorrhage associated with FUS-induced BBB opening in a rat model[11]. They compared SWI images acquired with a heavy T2*w gradient recalled 3D FLASH sequence to T2w images and found that SWI was more sensitive than T2w in detecting hemorrhages and monitoring the recovery process of damaged tissue after sonication. In 2009, the same group investigated the use of fully flow-compensated heavy T2*w imaging enhanced by super-paramagnetic iron oxide (SPIO) particles to differentiate FUS-induced BBB disruption from brain hemorrhage in rats[107]. BBB disruption was achieved using a FUS transducer with a frequency of 1.5 MHz and acoustic pressures ranging from 1.1 to 3.5 MPa. They found that T2*w images with and without SPIO injection could differentiate FUS-induced BBB opening from brain hemorrhage, suggesting that T2*w enhanced by SPIO might be more advantageous than contrast-enhanced T1-weighted images for detecting and delineating BBB opening.

Most studies assessing the safety of FUS-induced BBB opening combine T2w imaging with T2*w or SWI. T2w imaging is used to detect edema, while T2*w or SWI are employed to investigate brain hemorrhage[74,108,109]. An example of SWI images is shown in Fig. 5. To our knowledge, only one study assessed brain hemorrhage by using both T2*w and SWI[20], whereas most studies choose between T2*w and SWI to avoid redundant information and excessive acquisition time.

Some studies acquired T2w, T2*w, or SWI before sonication procedures to establish a baseline for comparison with post-FUS images[11,38]. However, most preclinical studies only used these sequences after sonication procedures. Imaging acquisitions can start 15 minutes after the sonication procedure (54) and continue up to 2 hours after[32]. MR-guided FUS systems offer the advantage of starting acquisitions immediately after the FUS procedure. While delays between the sonication procedure and MR acquisition are less critical for assessing safety compared to efficacy investigations, it is still relevant to investigate long-term safety. For this purpose, MR safety acquisitions can be repeated one day[20], 3 days[32], or 30 hours[13] after FUS procedures. In most cases, microhemorrhages and edema were not detected by imaging in the days following the sonication procedure with the acoustic parameters (US frequency, acoustic pressure, and MB concentration) used in these studies. A study reported some vascular adverse events following the FUS procedure; however, a scan performed a week later showed no hyperintense or hypointense voxels on T2w and SWI in the regions where they were previously observed[13].

Other sequences. In addition to T2w, T2*w and SWI previously described, several recent publications have assessed the safety of FUS-mediated BBB opening procedures using more sophisticated MR sequences, such as diffusion-weighted imaging (DWI)[20,29,31,38], DTI[41,109], arterial spin labeling (ASL)[12,29,41], or MR angiography (MRA)[84]. First applied by Tu et al. in 2020[109], DTI was combined with chemical exchange saturation transfer (CEST) imaging to investigate morphological and metabolic changes following FUS-mediated BBB opening in rats at 9.4 T. These sequences were acquired one day, two weeks, and six weeks after sonication to assess the effects of multiple weekly FUS procedures. They observed morphological changes in rats receiving multiple weekly FUS + MB treatments, indicated by hyperintense voxels in DTI images. In addition to DTI, Rigollet and colleagues measured cerebral blood flow (CBF) using a pulsed arterial spin labeling (pCASL) sequence (derived from ASL)[41]. They studied the dynamics of CBF after sonication in rats and noted a decrease in CBF immediately following FUS + MB procedures, Fig. 6. However, this vasoconstriction was transient, with CBF returning to baseline 90 minutes after sonication. A similar decrease in CBF in the sonicated region was observed by the same group[29]. To complement their MR protocol, they applied DWI to measure the apparent diffusion coefficient (ADC) to identify hyperintense or hypointense voxels and detect any microhemorrhages caused by the procedure. Additionally, the vascular anatomy of the primate brain was imaged using a 3D time-of-flight sequence at 3 T after FUS + MB procedures[84]. In this work, the authors did not detect any vascular damage in MRA images.

In conclusion, while T2w, T2*w, and SWI remain the primary sequences used to ensure the safety of FUS-induced BBB opening procedures, recent studies utilizing functional sequences to measure CBF or ADC have demonstrated their value in studying both the immediate and long-term vascular impacts of single or repeated sonication procedures.

Brain functionality

Since the beginning of FUS applications, there has been growing interest in how FUS can induce brain stimulation for clinical applications in psychiatry and neurology. Preclinical studies have demonstrated that FUS can be used for non-invasive cortical or subcortical brain stimulation, inducing either excitatory or inhibitory effects in the CNS, and even altering behavior in

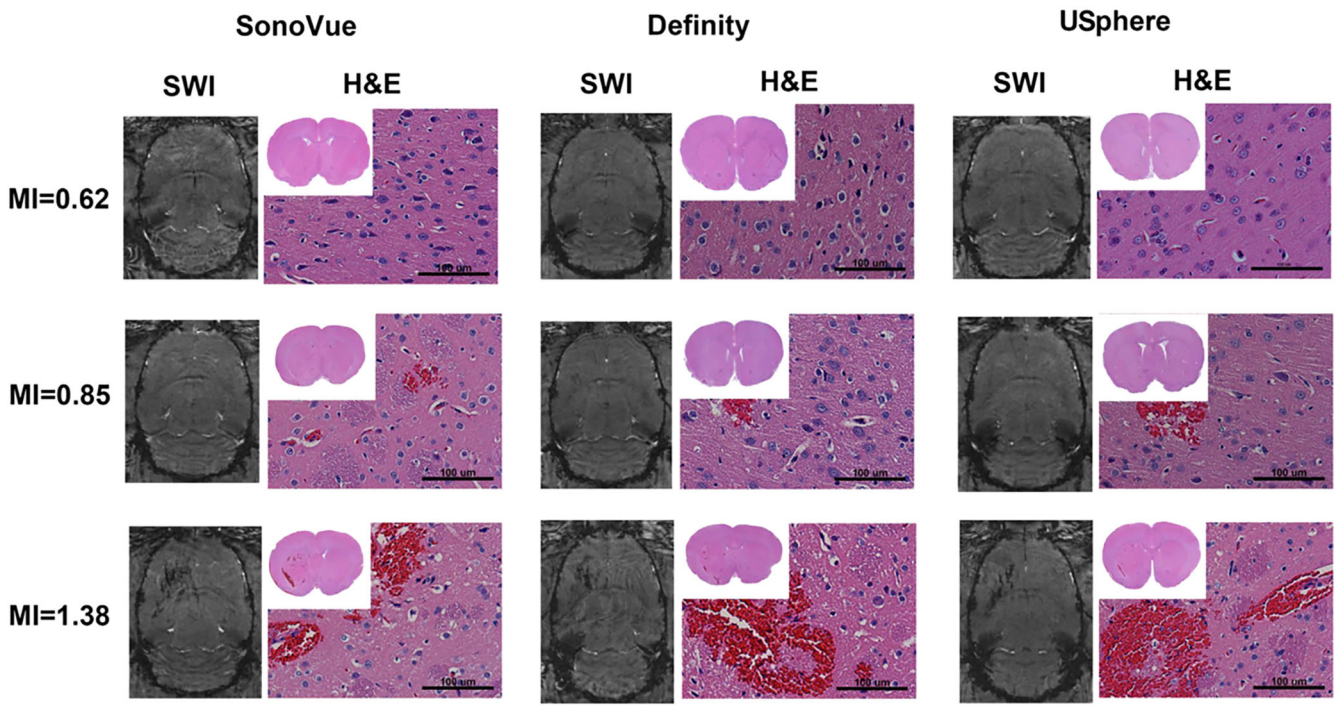

Fig. 5 | SWI images and their corresponding hematoxylin-eosin stained brain at different mechanical index levels for three kinds of microbubble administration. Exposure at 1.38 mechanical index caused a noticeable signal drop observed from SWI images. Figure reproduced with permission from ref. 53.

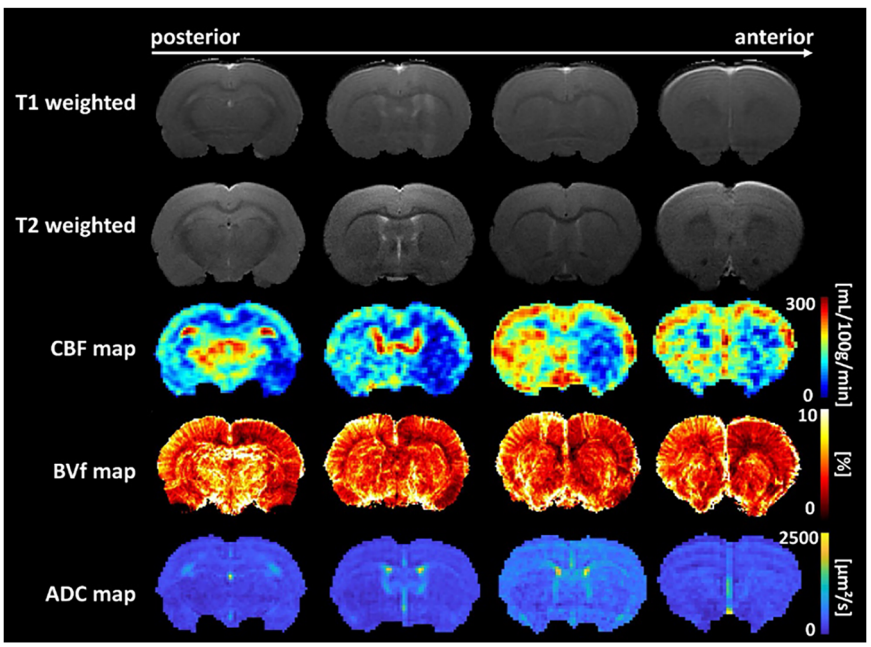

Fig. 6 | Representative MRI images (T1w, T2w, CBF map, blood volume fraction (BVf) map, ADC map) obtained from one animal after FUS-induced BBB disruption. Figure adapted with permission from ref. 41.

NHPs[110,111]. Functional MRI (fMRI), based on the blood oxygen level-dependent (BOLD) imaging technique, detects variations in the ratio of oxyhemoglobin to deoxyhemoglobin[112]. This technique relies on detecting changes in blood oxygenation and flow that occur in response to neural activity. When a specific brain region is more active, it consumes more oxygen, leading to localized changes in the concentration of deoxygenated hemoglobin. These changes alter the magnetic properties of the blood, which are detected by MRI.

In 2015, Chu and colleagues were the first to investigate the effects of FUS-mediated BBB opening procedures on neuronal activity[36]. They performed fMRI at 7 T on rats before sonication, one hour after, and at 2 days and 7 days post-procedure. They found that FUS-induced BBB opening was accompanied by reversible changes in neuronal responses. This reversibility was also observed by Todd et al.[12] using a transducer operating at 690 kHz and an acoustic pressure of 0.344 MPa. They noted that the neurovascular response to stimuli (such as stimulus-evoked fMRI and carbogen breathing gas challenge) was attenuated in both amplitude and duration in the region targeted by FUS-induced BBB opening. However, these effects resolved within 24 hours after sonication. The same group found that combining FUS-mediated BBB opening with GABA injection further reduced the peak amplitude and spatial extent of the BOLD signal response to the stimulus[113]. More recently, fMRI was used on

Table 3 | Type of radiotracers used to investigate FUS-mediated BBB opening safety and efficacy in preclinical studies

Assessment	Animals	Radiotracers
Neuroinflammation	Mice	^{18}F-FDG[61], ^{18}F-DPA-714[82]
	Rats	^{18}F-DPA-714[108]
BBB opening dynamic	Mice	^{64}Cu-AuNCs[63–65,85], ^{18}F-FDS[58,59], ^{18}F-FSPG[60], 3-^{11}C-AIB[56]
	Rats	^{18}F-fluoro-L-phenylalanine-fructose[55], ^{11}C-erlotinib[74], ^{11}C-metoclopramide[21]
Pharmacokinetic	Mice	^{68}Ga-bevacizumab[57], ^{11}C-topotecan[60], ^{89}Zr-mCD47[33], ^{64}Cu-AAV9[80], ^{18}F-DASA-10 [96], ^{89}Zr-DFO-C4[59], ^{89}Zr-CTX[82]
	Rats	^{18}F-FDG[62]
	Non-human primate	^{18}F-Choline[20]

NHPs at 3 T after FUS + MB procedures[114]. The authors observed that applying FUS to deep brain structures can alter functional connectivity in major brain networks, such as the default mode network and the frontotemporal network.

Neuroinflammation

FUS-induced BBB opening has been associated with some evidence of inflammation[115]. Due to its ability to measure specific proteins at low concentrations, PET is particularly well-suited for quantifying neuroinflammation and has the potential to discriminate among components of the neuroimmune response[116](Table 3). In contrast, MRI cannot directly visualize the inflammatory changes associated with FUS + MB treatment. PET can non-invasively investigate neuroinflammation by targeting the translocator protein (TSPO), an outer mitochondrial membrane receptor known to be upregulated in activated microglia and macrophages[117]. To investigate neuroinflammatory changes, Sinharay et al. proposed using PET imaging with [18F]-DPA714 as a biomarker of TSPO to assess neuroinflammation following single and multiple sonication procedures. They found that [18F]-DPA714 binding was increased in the sonicated region compared to the non-sonicated brain when PET was performed 40 minutes after FUS + MB. Additionally, they did not observe a cumulative increase in neuroinflammation on PET in rats imaged after two or six sonication procedures. The same radiotracer was used by Porret et al. to assess neuroinflammation in mice bearing glioblastoma[82]. They acquired 60-minute PET images 48 hours after intravenous injection of 250 MBq of [18F]-DPA714 following sonication procedures. In another study, Bastiancich and colleagues proposed using [18F]-FDG (5 MBq injected intravenously) as a radiotracer for neuroinflammation[61]. PET imaging was applied to mice with orthotopic glioblastoma 48 hours after FUS-induced BBB opening procedures. They did not find evidence of neuroinflammation 48 hours after sonication.

Transposition to clinical application

Several methods have been developed preclinically to perform FUS-induced BBB opening. In 2016, a system was proposed to implant MR-compatible single-element transducers in the heads of NHPs using a 10-mm flat piezoceramic disk[31]. This setup led to the publication of the first clinical trial involving FUS procedures in humans[95]. Another setup, based on MR-guided FUS initially developed in rabbits[86], was subsequently translated to clinical applications[88]. More recently, a clinical adaptation of the neuronavigation setup used to guide FUS[17] was performed in patients with glioblastoma[118]. The safety and efficacy of these systems were first tested preclinically before their clinical application. Imaging sequences were then adapted to meet practical clinical constraints, such as reasonable acquisition times, device availability, and cost. As a result, more streamlined protocols were developed to address these limitations. These protocols included a limited number of acquisitions (Tables 4, 5), using only the imaging sequences essential for assessing safety and efficacy.

Table 4 | MR sequences used in clinical to evaluate the safety of the FUS procedure

Sequence	1.5 T	3 T
T2w	-	122,130,131
T2*w	118	88,123,126,128,129,131–135,138–140,142,143,193
SWI	118	20,95,123,124,127,130,134,136,137,141
FLAIR		19,20,95,122,124,127–129,133–138,140
Thermometry	-	88,122,123
DWI	-	19,20,95,122,129,130,138,140

T2w T2-weighted, *SWI* Susceptibility weighted imaging, *FLAIR* Fluid-attenuated inversion recovery, *DWI* Diffusion weighted imaging, *T1w-DCE* T1-weighted dynamic contrast-enhanced.

Table 5 | MR sequences applied in clinical to investigate the efficacy of the FUS-mediated BBB opening procedure

Sequence	1.5 T	3 T
T1w-CE	118	19,20,88,95,119–124,126–143,193
T1w-DCE	118	176
T2*w	–	126
SWI	–	130

T1w-CE T1-weighted contrast-enhanced, *T1w-CE* T1-weighted dynamic contrast-enhanced, *T2*w* T2*-weighted, *SWI* susceptibility weighted imaging.

Ensuring safety

Except of three studies, where safety was not evaluated because the setup and acoustic parameters had been previously validated[119–121], imaging is used to ensure the safety of the sonication procedure. As the MRgFUS setup has been translated to clinical settings, the thermometry sequences used preclinically in such systems were then applied clinically to monitor tissue temperature during FUS procedures[88,122,123]. This sequence is the primary MR technique for sonication monitoring; however, a recent publication proposed the use of ultrasound imaging for monitoring FUS + MB[124]. The study demonstrated the potential of PAM (registered with B-mode or MR images) to effectively monitor the sonication process.

Most imaging sequences are performed after sonication procedures to detect potential adverse events. Similar to preclinical studies, T2w (or FLAIR), T2*w, and SWI sequences are predominantly used to assess the safety of FUS-mediated BBB opening procedures (Table 4) by detecting the presence of edema (T2w, FLAIR) and hemorrhage (T2*w and SWI). Unlike in preclinical studies, T2*w is the primary sequence applied, followed by T2w (or FLAIR) and SWI, reported in 60%, 53%, and 40% of the studies, respectively. The use of the FLAIR sequence is notable, as FLAIR has a longer echo time and repetition time than traditional T2w, making it easier to detect abnormalities, which remain hyperintense while cerebrospinal fluid flow appears hypointense[125].

Interestingly, compared to preclinical studies, DWI is frequently used to assess the safety of FUS-mediated BBB opening. Indeed, 27% of the studies report the use of DWI to specifically investigate the presence of ischemia[95].

To investigate safety, 53% of the studies reported a baseline acquisition of safety sequences. When specified, baseline acquisitions were performed 1–2 days before the procedure[95,126,127], one week before[128], or one month prior[123,124,129]. Additionally, Chang and colleagues adjusted the baseline timing based on the patient's condition: one week for glioblastoma and one month for patients with Alzheimer's disease[130]. MR acquisitions were then performed immediately after the procedure in every study assessing sonication. Long-term safety assessments were conducted at various time points: one day[88,118,122,123,128,129,131–137], two to three days[124,134], one week[88,122,128,134,138], two weeks[129,136,137], one month[88,122,123,126], two months[88,130], and up to three months[124,129,138,139] after the last procedures. Moreover, two studies reported MR safety assessments at 8 months and one year after the last FUS procedure in patients with Alzheimer's disease[135,140]. Most studies did not report any adverse events based on MR safety assessments. When hypo-intensities were detected on SWI images[118,123,129] they can persist up to two or three months[123,129].

The use of ultrasound imagingstudies has also been reported in safety investigations, as previously reported[124]. As well as PET imaging is a suitable imaging device to investigate the safety of the patient after the FUS+MBs procedure[140]. In PET, [18 F]-fluorodeoxyglucose has been used to investigate the potential neuroinflammation effect after BBB disruption, and no adverse events were reported[140].

Efficacy assessment

Compared to safety investigations performed using MRI, efficacy was assessed in every publication related to FUS + MB clinical trials. Each publication associated with clinical FUS-mediated BBB opening procedures included the acquisition of T1w-CE images to assess BBB permeabilization, Fig. 7. Pre-contrast-enhanced T1w images were acquired as a baseline before FUS treatment in 63% of studies related to FUS + MB clinical trials. Where reported, baseline T1w-CE images were acquired 1–2 days[95,121,126,127,136,141] (6 publications), one week[119,128,130] (3 publications) or one month[123,124,129,130,134] (5 publications) before FUS procedures. After the sonication procedure, T1w-CE images were acquired as soon as possible, depending on the time required to transfer the patient from the FUS system to the MR scanner. The shortest time reported in the literature between the sonication procedure and T1w-CE acquisition was 10 minutes, with the contrast agent injected immediately after the MBs[95,127]. On average, T1w-CE images were acquired 55 minutes later (ranging from 15 minutes[132] to 2 hours[124]) as reported[121,124,132,136,140–143], with gadolinium contrast-agent such as Dotarem[95,127], Gadovist[118], diethylene-triamine pentaacetic acid[129] or Gadovist[137] injected 10-30 minutes before T1w-CE acquisition[124,129,134,137,140,141].

Finally, the reversibility of BBB opening was investigated in 77% of the studies. Reversibility was most often assessed 24 hours after sonication procedures (in 53% of the studies). If BBB permeabilization was still observed on MRI, a follow-up T1w-CE acquisition was performed 2–3 days after sonication[128,133,134]. Long-term reversibility was then assessed using T1w-CE acquisitions performed from two weeks to three months after sonication[130,137,139].

In addition to T1w-CE, other sequences have been explored, such as T1w-DCE, where kinetic parameters were evaluated using dynamic contrast-enhanced T1w-Gd to characterize the kinetic behavior of the FUS target[118]. Moreover, Park et al. demonstrated that combining T2*w images

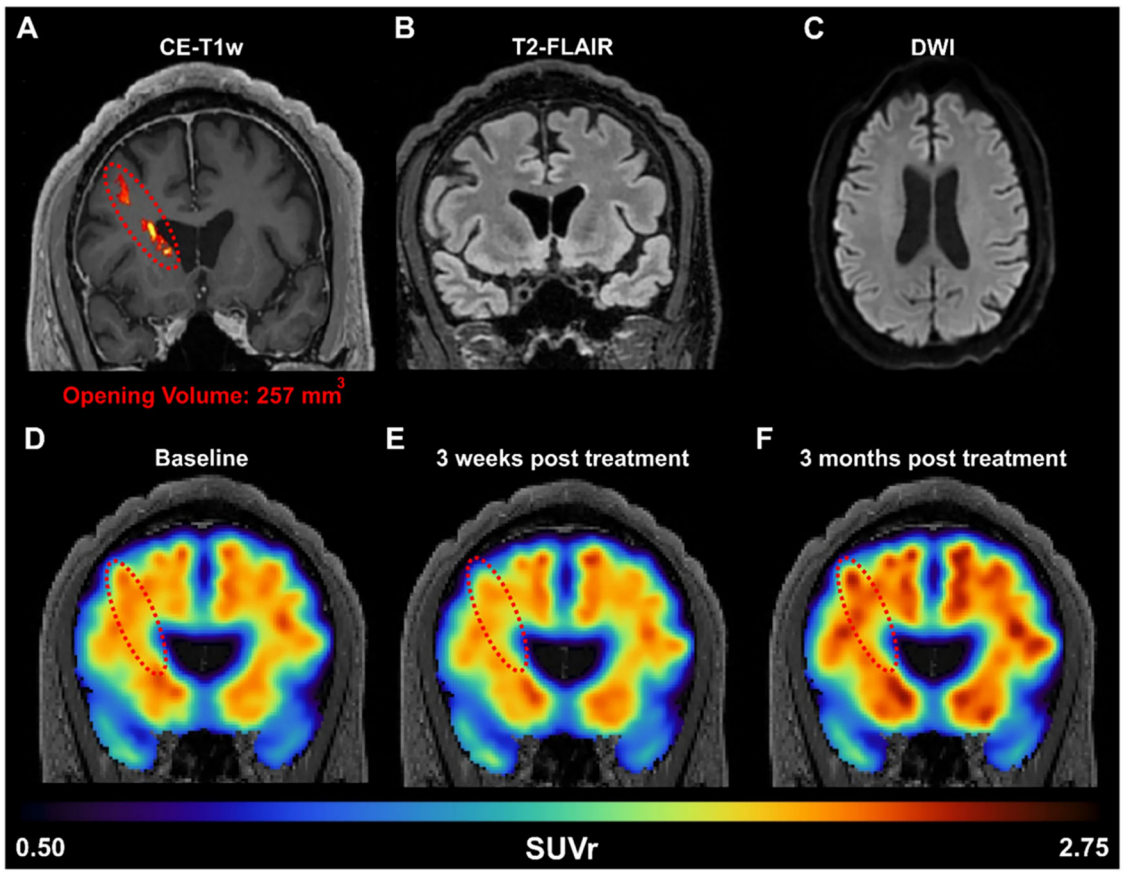

Fig. 7 | Clinial MR sequences acquired after FUS-mediated BBB opening and amyloid PET imaging acquired before and after sonication in a patient. **A** Amyloid PET signal reduction following FUS treatment in an early AD patient. BBB opening in the right prefrontal cortex was confirmed immediately after FUS exposure through contrast-enhanced T1-weighted (CE-T1w) MRI, revealing a contrast enhancement volume of 257 mm3 (red dotted oval). MRI safety scans, acquired on the day of treatment, including (**B**) T2-FLAIR and (**C**) DWI, indicate a safe opening without edema or hemorrhaging. The amyloid PET signal was measured at the (**D**) baseline pre-FUS, **E** 3 weeks, and (**F**) 3 months post-FUS. Within the treated frontal lobe, we detected a reduction of 1.8% in the SUVr 3 weeks after treatment, followed by a 5.9% increase in SUVr 3 months after treatment, all relative to the baseline scan. Figure reproduced with permission from ref. 19.

Table 6 | Type of radiotracers used to investigate FUS-mediated BBB opening safety and efficacy in clinical studies

Assessment	Pathology	Radiotracers
β-amyloid deposition	Alzheimer	^{18}F-Florbetaben[88,119,133,135,139], ^{18}F-Fluorobetapir[124,140]
	Parkinson	^{18}F-Florbetaben[123,129], ^{18}F-Flutemetamol[123], ^{18}F-Fluorodopa[129]
Glucose metabolism	Alzheimer	^{18}F-FDG[140]
	Parkinson	^{18}F-FDG[123,138]
Pharmacokinetic	Parkinson	^{18}F-Choline[137]

with T1w-CE images provided better sensitivity for assessing BBB permeability than T1w-CE alone[126]. In addition, Chang and colleagues observed that low signal intensities on SWI also indicated BBB opening[130].

PET imaging in beta amyloid. Several studies have demonstrated the potential of PET to assess the efficacy of sonication procedures, particularly in patients with Alzheimer's and Parkinson's diseases. Preclinical studies have shown that FUS-mediated BBB opening can reduce amyloid extracellular deposition in mice with Alzheimer's disease[144,145]. This effect against Alzheimer's pathology appears to be enhanced by the concomitant delivery of antibodies against β-amyloid and tau, leading to improved cognitive performance in mice. Furthermore, Alzheimer's pathology is prevalent in Parkinson's disease with dementia, and striatal β-amyloid accumulation is more common in Parkinson's patients with dementia than in those without dementia. Therefore, several studies have explored FUS-mediated BBB opening to investigate amyloid deposition in patients with Alzheimer's or Parkinson's disease.

Different radiotracers have been used to observe reductions in β-amyloid deposition in patients with Alzheimer's and Parkinson's diseases (Table 6). For example, [18 F]-Florbetaben was injected, and PET imaging was performed one week[133], one month[123], two months[88,119], three months[129,139], or 6-12[135] months after FUS treatment. While the first study in Alzheimer's patients did not observe any reduction in β-amyloid deposition after FUS + MB procedures[88], later studies reported reductions in β-amyloid in both Alzheimer's and Parkinson's patients[129,133]. Specifically, for Alzheimer's patients, the [18 F]-Fluorobetapir radiotracer was evaluated to assess decreases in amyloid burden near the targeted FUS area[124,140], Fig. 7. PET imaging acquisitions were performed 3–8 months after FUS treatment, with only one study observing a decrease in β-amyloid deposition[124].

In Parkinson's disease, [18 F]-Flutemetamol[123] and [18 F]-Fluorodopa[129] were used. Sensitive results with [18 F]-Fluorodopa suggested a β-amyloid-lowering effect in the treated putamen region, whereas no changes were detected with [18 F]-Flutemetamol. Other studies in Parkinson's patients used PET imaging with [18 F]-fluorodeoxyglucose to assess glucose metabolism, as glucose metabolism impairment is associated with Alzheimer's and Parkinson's diseases[123,138,140]. Unlike the studies by Gasca-Salas et al.[123] and Epelbaum et al.[140], Meng and colleagues observed a reduction in the standardized uptake value ratio on fluorodeoxyglucose PET imaging in the treated putamen region[138]. Finally, a recent study using [18 F]-Choline, showed an improvement in drug uptake after FUS treatments in Parkinson's patients[137].

Future perspectives and conclusion

In summary, FUS-mediated BBB disruption is emerging as an innovative approach to treat various neurological disorders. The technique has demonstrated both efficacy and safety in extensive preclinical studies and preliminary clinical trials. As highlighted in this review, MRI has primarily been used to assess the efficacy and safety of FUS + MB procedures, more so than nuclear or ultrasound imaging. Most studies evaluated efficacy with MR contrast agents and T1w contrast-enhanced sequences immediately following sonication, while T2w or T2*w MR sequences were used up to two days after FUS + MB to investigate safety. PET imaging, though less frequently used compared to MRI, is a powerful method with reliable radiotracers for studying neuroinflammation, efflux pump function, and monitoring drug delivery. Although ultrasound is used less frequently than MRI and nuclear imaging, recent studies highlight the value of PAM for providing simultaneous safety and efficacy assessments during FUS procedures.

Future perspectives

Further work is required to refine optimal parameters and minimize risks such as hemorrhage, edema, or ineffective therapeutic doses. Some studies have used functional MRI to investigate neurovascular, functional, and neuromodulatory changes induced by the FUS + MB procedure. Additional research using functional MRI is needed, particularly in Alzheimer's disease, to evaluate cognitive improvements after sonication or to assess neuroplasticity and regeneration associated with gliosis reactivation following FUS[146,147].

More sophisticated sequences, such as ASL, have been used to provide quantitative vascular assessments, which are more informative than the qualitative insights provided by T2w images. These sequences can evaluate the impact of FUS-mediated BBB opening on CNS hemodynamics[41]. Future studies should focus on vascular perfusion to identify inflammation biomarkers applicable to clinical settings. PET imaging remains a reliable technique for investigating neuroinflammatory effects potentially induced by FUS, and it holds promise for quantitatively assessing molecular effects of sonication, optimizing the therapeutic window with both established and novel P-gp radiotracers.

The efficacy of FUS-mediated BBB opening is typically assessed using T1w imaging following the administration of a gadolinium-based contrast agent, which remains the standard in current practice. Although gadolinium has an established safety profile, there are emerging concerns about its toxicity and tissue retention, which can affect pediatric patients and subjects with renal impairment[148,149]. Alternative imaging methods have been proposed to replace gadolinium contrast agents. DTI-based assessment using fractional anisotropy maps has shown encouraging results as a contrast-free imaging alternative in non-human primate models[38]. Nonetheless, additional preclinical and clinical studies are necessary to confirm its translational relevance. Other MR imaging methods have also been introduced to replace gadolinium-based contrast agents, such as manganese-based contrast agents[150] or ASL as a contrast-free technique focused on the quantitative measurement of tissue perfusion[151]. However, these techniques still need to be investigated in the context of FUS-mediated BBB opening studies.

Both nuclear imaging and MRI have limitations, including a lack of portability and the inability to monitor safety and efficacy in real-time during FUS procedures. Ultrasound imaging, with its high temporal resolution and portability, could address these challenges. Although signal aberration caused by the skull limits the use of ultrasound in brain imaging, recent studies have shown promise in using ultrasound for both safety and efficacy assessments. Preclinical and clinical studies have demonstrated that PAM is a relevant method for real-time visualization of cavitation activity[75,124] providing simultaneous evaluations of efficacy and safety during FUS procedures. Further research on PAM is needed, particularly with the use of matrix array probes for 3D PAM to provide more comprehensive volumetric cavitation information.

Additionally, skull aberration correction algorithms are necessary to improve cavitation mapping. To correct for skull-induced acoustic aberrations, computed tomography (CT) is typically employed to estimate the skull density ratio, skull volume, and generate patient-specific maps of acoustic properties. However, CT imaging introduces additional procedural time and exposes patients to ionizing radiation. To address these limitations, ultra-short echo time (UTE) and zero echo time (ZTE) MRI sequences have been proposed as alternatives to generate pseudo-CT images[152,153]. Although these MRI-based techniques have primarily been investigated in vitro using human skulls, emerging evidence suggests their potential to replace conventional CT scans in this context[154].

Finally, despite the significant technological advancements in FUS over the past 20 years in preclinical studies, clinical applications of FUS-mediated BBB opening are only just beginning. Clinical optimization is needed to standardize FUS-mediated BBB opening as a treatment modality, with imaging methods tailored to meet clinical demands.

Data availability

No datasets were generated or analysed during the current study.

Received: 22 April 2025; Accepted: 7 August 2025;
Published online: 01 October 2025

References

1. Taylor, E. M. The impact of efflux transporters in the brain on the development of drugs for CNS disorders. *Clin. Pharmacokinet.* **41**, 81–92 (2002).
2. Konofagou, E. E. et al. Ultrasound-induced blood-brain barrier opening. *Curr. Pharm. Biotechnol.* **13**, 1332–1345 (2012).
3. Burgess, A., Shah, K., Hough, O. & Hynynen, K. Focused ultrasound-mediated drug delivery through the blood-brain barrier. *Expert Rev. Neurother.* **15**, 477–491 (2015).
4. Jordão, J. F. et al. Antibodies targeted to the brain with image-guided focused ultrasound reduces amyloid-beta plaque load in the TgCRND8 mouse model of Alzheimer's disease. *PLoS One* **5**, e10549 (2010).
5. Liu, H. L. et al. Magnetic resonance monitoring of focused ultrasound/magnetic nanoparticle targeting delivery of therapeutic agents to the brain. *Proc. Natl. Acad. Sci. USA* **107**, 15205–15210 (2010).
6. Hsu, P. H. et al. Noninvasive and targeted gene delivery into the brain using microbubble-facilitated focused ultrasound. *PLoS One* **8**, e57682 (2013).
7. Tung, Y. S., Vlachos, F., Feshitan, J. A., Borden, M. A. & Konofagou, E. E. The mechanism of interaction between focused ultrasound and microbubbles in blood-brain barrier opening in mice. *J. Acoust. Soc. Am.* **130**, 3059–3067 (2011).
8. Fisher, D. G. & Price, R. J. Recent advances in the use of focused ultrasound for magnetic resonance image-guided therapeutic nanoparticle delivery to the central nervous system. *Front Pharm.* **10**, 1348 (2019).
9. Marty, B. et al. Dynamic study of blood-brain barrier closure after its disruption using ultrasound: a quantitative analysis. *J. Cereb. Blood Flow. Metab.* **32**, 1948–1958 (2012).
10. Chen, H. & Konofagou, E. E. The size of blood-brain barrier opening induced by focused ultrasound is dictated by the acoustic pressure. *J. Cereb. Blood Flow. Metab.* **34**, 1197–1204 (2014).
11. Liu, H. L. et al. Hemorrhage detection during focused-ultrasound-induced blood-brain-barrier opening by using susceptibility-weighted magnetic resonance imaging. *Ultrasound Med Biol.* **34**, 598–606 (2008).
12. Todd, N., Zhang, Y., Livingstone, M., Borsook, D. & McDannold, N. The neurovascular response is attenuated by focused ultrasound-mediated disruption of the blood-brain barrier. *Neuroimage* **201**, 116010 (2019).
13. Downs, M. E. et al. Long-term safety of repeated blood-brain barrier opening via focused ultrasound with microbubbles in non-human primates performing a cognitive task. *PLoS One* **10**, e0125911 (2015).
14. Hynynen, K., McDannold, N., Vykhodtseva, N. & Jolesz, F. A. Noninvasive MR imaging-guided focal opening of the blood-brain barrier in rabbits. *Radiology* **220**, 640–646 (2001).
15. Arif, W. M. et al. Focused ultrasound for opening blood-brain barrier and drug delivery monitored with positron emission tomography. *J. Control Release* **324**, 303–316 (2020).
16. McDannold, N., Vykhodtseva, N. & Hynynen, K. Effects of acoustic parameters and ultrasound contrast agent dose on focused-ultrasound induced blood-brain barrier disruption. *Ultrasound Med. Biol.* **34**, 930–937 (2008).
17. Wei, K. C. et al. Neuronavigation-guided focused ultrasound-induced blood-brain barrier opening: a preliminary study in swine. *AJNR Am. J. Neuroradiol.* **34**, 115–120 (2013).
18. Tournier, N., Comtat, C., Lebon, V. & Gennisson, J. L. Challenges and Perspectives of the Hybridization of PET with Functional MRI or Ultrasound for Neuroimaging. *Neuroscience* **474**, 80–93 (2021).
19. Karakatsani, M. E. et al. Focused ultrasound mitigates pathology and improves spatial memory in Alzheimer's mice and patients. *Theranostics* **13**, 4102–4120 (2023).
20. Blesa, J. et al. BBB opening with focused ultrasound in nonhuman primates and Parkinson's disease patients: Targeted AAV vector delivery and PET imaging. *Sci. Adv.* **9**, eadf4888 (2023).
21. Goutal, S. et al. Imaging the impact of blood-brain barrier disruption induced by focused ultrasound on P-glycoprotein function. *J. Control Release* **361**, 483–492 (2023).
22. Karakatsani, M. E. M., Samiotaki, G. M., Downs, M. E., Ferrera, V. P. & Konofagou, E. E. Targeting effects on the volume of the focused ultrasound-induced blood-brain barrier opening in nonhuman primates in vivo. *IEEE Trans. Ultrason Ferroelectr. Freq. Control* **64**, 798–810 (2017).
23. Samiotaki, G., Vlachos, F., Tung, Y. S. & Konofagou, E. E. A quantitative pressure and microbubble-size dependence study of focused ultrasound-induced blood-brain barrier opening reversibility in vivo using MRI. *Magn. Reson. Med.* **67**, 769–777 (2012).
24. Kamimura, H. A. et al. Chirp- and random-based coded ultrasonic excitation for localized blood-brain barrier opening. *Phys. Med Biol.* **60**, 7695–7712 (2015).
25. Choi, J. J., Selert, K., Vlachos, F., Wong, A. & Konofagou, E. E. Noninvasive and localized neuronal delivery using short ultrasonic pulses and microbubbles. *Proc. Natl. Acad. Sci. USA* **108**, 16539–16544 (2011).
26. Tung, Y. S. et al. In vivo transcranial cavitation threshold detection during ultrasound-induced blood-brain barrier opening in mice. *Phys. Med. Biol.* **55**, 6141–6155 (2010).
27. Aryal, M. et al. MRI monitoring and quantification of ultrasound-mediated delivery of liposomes dually labeled with Gadolinium and Fluorophore through the Blood-Brain Barrier. *Ultrasound Med. Biol.* **45**, 1733–1742 (2019).
28. Conti, A. et al. Empirical and theoretical characterization of the diffusion process of different Gadolinium-based nanoparticles within the brain tissue after ultrasound-induced permeabilization of the blood-brain barrier. *Contrast Media Mol. Imaging* **2019**, 6341545 (2019).
29. Labriji, W. et al. Evidence of cerebral hypoperfusion consecutive to ultrasound-mediated blood-brain barrier opening in rats. *Magn. Reson. Med* **89**, 2281–2294 (2023).
30. Conti, A., Mériaux, S. & Larrat, B. About the Marty model of blood-brain barrier closure after its disruption using focused ultrasound. *Phys. Med Biol.* **64**, 14nt02 (2019).
31. Goldwirt, L. et al. Enhanced brain distribution of carboplatin in a primate model after blood-brain barrier disruption using an implantable ultrasound device. *Cancer Chemother. Pharm.* **77**, 211–216 (2016).
32. Pouliopoulos, A. N. et al. A clinical system for non-invasive blood-brain barrier opening using a neuronavigation-guided single-element focused ultrasound transducer. *Ultrasound Med Biol.* **46**, 73–89 (2020).
33. Sheybani, N. D. et al. ImmunoPET-informed sequence for focused ultrasound-targeted mCD47 blockade controls glioma. *J. Control Release* **331**, 19–29 (2021).
34. Choi, H., Lee, E. H., Han, M., An, S. H. & Park, J. Diminished Expression of P-glycoprotein using focused ultrasound is

associated with JNK-dependent signaling pathway in cerebral blood vessels. *Front. Neurosci.* **13**, 1350 (2019).
35. Noel, R. L. et al. Natural aging and Alzheimer's disease pathology increase susceptibility to focused ultrasound-induced blood-brain barrier opening. *Sci. Rep.* **13**, 6757 (2023).
36. Chu, P. C. et al. Neuromodulation accompanying focused ultrasound-induced blood-brain barrier opening. *Sci. Rep.* **5**, 15477 (2015).
37. Magnin, R. et al. Magnetic resonance-guided motorized transcranial ultrasound system for blood-brain barrier permeabilization along arbitrary trajectories in rodents. *J. Ther. Ultrasound* **3**, 22 (2015).
38. Karakatsani, M. E., Pouliopoulos, A. N., Liu, M., Jambawalikar, S. R. & Konofagou, E. E. Contrast-free detection of focused ultrasound-induced blood-brain barrier opening using diffusion tensor imaging. *IEEE Trans. Biomed. Eng.* **68**, 2499–2508 (2021).
39. Samiotaki, G. & Konofagou, E. E. Dependence of the reversibility of focused- ultrasound-induced blood-brain barrier opening on pressure and pulse length in vivo. *IEEE Trans. Ultrason Ferroelectr. Freq. Control* **60**, 2257–2265 (2013).
40. Wu, S. Y. et al. Efficient blood-brain barrier opening in primates with neuronavigation-guided ultrasound and real-time acoustic mapping. *Sci. Rep.* **8**, 7978 (2018).
41. Rigollet, S. et al. FUS-mediated BBB opening leads to transient perfusion decrease and inflammation without acute or chronic brain lesion. *Theranostics* **14**, 4147–4160 (2024).
42. Chai, W. Y. et al. Magnetic-resonance imaging for kinetic analysis of permeability changes during focused ultrasound-induced blood-brain barrier opening and brain drug delivery. *J. Control Release* **192**, 1–9 (2014).
43. Marquet, F., Tung, Y. S., Teichert, T., Ferrera, V. P. & Konofagou, E. E. Noninvasive, transient and selective blood-brain barrier opening in non-human primates in vivo. *PLoS One* **6**, e22598 (2011).
44. Choi J. J., Pernot M., Small S. A., Konofagou E. E. Feasibility of transcranial, localized drug-delivery in the brain of Alzheimer's-model mice using focused ultrasound. In *IEEE Proceedings of Ultrasonics, Ferroelectrics and Frequency Quality Control* (2005).
45. Sun, T. et al. Acoustic cavitation-based monitoring of the reversibility and permeability of ultrasound-induced blood-brain barrier opening. *Phys. Med. Biol.* **60**, 9079–9094 (2015).
46. Baseri, B., Choi, J. J., Tung, Y. S. & Konofagou, E. E. Multi-modality safety assessment of blood-brain barrier opening using focused ultrasound and definity microbubbles: a short-term study. *Ultrasound Med. Biol.* **36**, 1445–1459 (2010).
47. Vlachos, F., Tung, Y. S. & Konofagou, E. Permeability dependence study of the focused ultrasound-induced blood-brain barrier opening at distinct pressures and microbubble diameters using DCE-MRI. *Magn. Reson. Med* **66**, 821–830 (2011).
48. Brix, L., Ringgaard, S. & Rasmusson, A. Three dimensional three component whole heart cardiovascular magnetic resonance velocity mapping: comparison of flow measurements from 3D and 2D acquisitions. *J. Cardiovasc. Magn. Reson.* **11**, 3 (2009).
49. Tofts, P. S. & Kermode, A. G. Measurement of the blood-brain barrier permeability and leakage space using dynamic MR imaging. 1. Fundamental concepts. *Magn. Reson/ Med/* **17**, 357–367 (1991).
50. Samiotaki, G. et al. Pharmacokinetic analysis and drug delivery efficiency of the focused ultrasound-induced blood-brain barrier opening in non-human primates. *Magn. Reson/ Imaging* **37**, 273–281 (2017).
51. Wu, S. Y. et al. Transcranial cavitation detection in primates during blood-brain barrier opening—a performance assessment study. *IEEE Trans. Ultrason/ Ferroelectr. Freq. Control* **61**, 966–978 (2014).
52. Yoon, K. et al. Localized blood-brain barrier opening in ovine model using image-guided transcranial focused ultrasound. *Ultrasound Med Biol.* **45**, 2391–2404 (2019).
53. Wu, S. K. et al. Characterization of different microbubbles in assisting focused ultrasound-induced blood-brain barrier opening. *Sci. Rep.* **7**, 46689 (2017).
54. Choi, J. J., Pernot, M., Small, S. A. & Konofagou, E. E. Noninvasive, transcranial and localized opening of the blood-brain barrier using focused ultrasound in mice. *Ultrasound Med. Biol.* **33**, 95–104 (2007).
55. Yang, F. Y. et al. Pharmacokinetic analysis and uptake of 18F-FBPA-Fr after ultrasound-induced blood-brain barrier disruption for potential enhancement of boron delivery for neutron capture therapy. *J. Nucl. Med.* **55**, 616–621 (2014).
56. Okada, M. et al. In-vivo imaging of blood-brain barrier permeability using positron emission tomography with 2-amino-[3-11C] isobutyric acid. *Nucl. Med. Commun*. **36**, 1239–1248 (2015).
57. Liu, H. L. et al. Focused ultrasound enhances central nervous system delivery of bevacizumab for malignant glioma treatment. *Radiology* **281**, 99–108 (2016).
58. Hugon, G. et al. [(18)F]2-Fluoro-2-deoxy-sorbitol PET imaging for quantitative monitoring of enhanced blood-brain barrier permeability induced by focused ultrasound. *Pharmaceutics* **13**, 1752 (2021).
59. Chevaleyre, C. et al. Efficient PD-L1 imaging of murine glioblastoma with FUS-aided immunoPET by leveraging FcRn-antibody interaction. *Theranostics* **13**, 5584–5596 (2023).
60. Molotkov, A. et al. Real-Time Positron Emission Tomography evaluation of topotecan brain kinetics after ultrasound-mediated blood-brain barrier permeability. *Pharmaceutics* **13**, 405 (2021).
61. Bastiancich, C. et al. Molecular imaging of ultrasound-mediated blood-brain barrier disruption in a mouse orthotopic Glioblastoma Model. *Pharmaceutics* **14**, 2227 (2022).
62. Yang, F. Y., Chang, W. Y., Chen, J. C., Lee, L. C. & Hung, Y. S. Quantitative assessment of cerebral glucose metabolic rates after blood-brain barrier disruption induced by focused ultrasound using FDG-MicroPET. *Neuroimage* **90**, 93–98 (2014).
63. Sultan, D. et al. Focused ultrasound enabled trans-blood brain barrier delivery of gold nanoclusters: effect of surface charges and quantification using Positron Emission Tomography. *Small* **14**, e1703115 (2018).
64. Ye, D. et al. Focused ultrasound-enabled delivery of radiolabeled nanoclusters to the pons. *J. Control Release* **283**, 143–150 (2018).
65. Ye, D. et al. Focused ultrasound combined with microbubble-mediated intranasal delivery of gold nanoclusters to the brain. *J. Control Release* **286**, 145–153 (2018).
66. Singh, A. et al. Guiding and monitoring focused ultrasound mediated blood-brain barrier opening in rats using power Doppler imaging and passive acoustic mapping. *Sci. Rep.* **12**, 14758 (2022).
67. Pathan, N. & Shende, P. Tailoring of P-glycoprotein for effective transportation of actives across blood-brain-barrier. *J. Control Release* **335**, 398–407 (2021).
68. Abbott, N. J., Patabendige, A. A., Dolman, D. E., Yusof, S. R. & Begley, D. J. Structure and function of the blood-brain barrier. *Neurobiol. Dis.* **37**, 13–25 (2010).
69. Aryal, M. et al. Effects on P-Glycoprotein Expression after Blood-Brain Barrier Disruption Using Focused Ultrasound and Microbubbles. *PLoS One* **12**, e0166061 (2017).
70. Conti, A. et al. Regulation of P-glycoprotein and Breast Cancer Resistance Protein Expression Induced by Focused Ultrasound-Mediated Blood-Brain Barrier Disruption: A Pilot Study. *Int J. Mol. Sci.* **23**, 15488 (2022).
71. Cho, H. et al. Localized Down-regulation of P-glycoprotein by Focused Ultrasound and Microbubbles induced Blood-Brain Barrier Disruption in Rat Brain. *Sci. Rep.* **6**, 31201 (2016).
72. Adkins, C. E. et al. P-glycoprotein mediated efflux limits substrate and drug uptake in a preclinical brain metastases of breast cancer model. *Front Pharm.* **4**, 136 (2013).

73. Tournier, N., Stieger, B. & Langer, O. Imaging techniques to study drug transporter function in vivo. *Pharm. Ther.* **189**, 104–122 (2018).
74. Goutal, S. et al. Physical blood-brain barrier disruption induced by focused ultrasound does not overcome the transporter-mediated efflux of erlotinib. *J. Control Release* **292**, 210–220 (2018).
75. Bae, S., Liu, K., Pouliopoulos, A. N., Ji, R. & Konofagou, E. E. Real-time passive acoustic mapping with enhanced spatial resolution in neuronavigation-guided focused ultrasound for blood-brain barrier opening. *IEEE Trans. Biomed. Eng.* **70**, 2874–2885 (2023).
76. Gyöngy, M. & Coussios, C. C. Passive spatial mapping of inertial cavitation during HIFU exposure. *IEEE Trans. Biomed. Eng.* **57**, 48–56 (2010).
77. Lu, S. et al. Passive acoustic mapping of cavitation using eigenspace-based robust Capon beamformer in ultrasound therapy. *Ultrason Sonochem.* **41**, 670–679 (2018).
78. Kamimura, H. A. S. et al. Real-time passive acoustic mapping using sparse matrix multiplication. *IEEE Trans. Ultrason Ferroelectr. Freq. Control* **68**, 164–177 (2021).
79. Jones, R. M., McMahon, D. & Hynynen, K. Ultrafast three-dimensional microbubble imaging in vivo predicts tissue damage volume distributions during nonthermal brain ablation. *Theranostics* **10**, 7211–7230 (2020).
80. Ajenjo, J. et al. PET imaging of focused-ultrasound enhanced delivery of AAVs into the murine brain. *Theranostics* **13**, 5151–5169 (2023).
81. Tran, V. L. et al. Impact of blood-brain barrier permeabilization induced by ultrasound associated to microbubbles on the brain delivery and kinetics of cetuximab: An immunoPET study using (89) Zr-cetuximab. *J. Control Release* **328**, 304–312 (2020).
82. Porret, E. et al. Refining the delivery and therapeutic efficacy of cetuximab using focused ultrasound in a mouse model of glioblastoma: An (89)Zr-cetuximab immunoPET study. *Eur. J. Pharm. Biopharm.* **182**, 141–151 (2023).
83. Valdez, M. A., Fernandez, E., Matsunaga, T., Erickson, R. P. & Trouard, T. P. Distribution and diffusion of macromolecule delivery to the brain via focused ultrasound using magnetic resonance and multispectral fluorescence imaging. *Ultrasound Med. Biol.* **46**, 122–136 (2020).
84. Wu, S. Y. et al. Characterizing focused-ultrasound mediated drug delivery to the heterogeneous primate brain in vivo with acoustic monitoring. *Sci. Rep.* **6**, 37094 (2016).
85. Yang, Y. et al. Cavitation dose painting for focused ultrasound-induced blood-brain barrier disruption. *Sci. Rep.* **9**, 2840 (2019).
86. Hynynen, K. et al. 500-element ultrasound phased array system for noninvasive focal surgery of the brain: a preliminary rabbit study with ex vivo human skulls. *Magn. Reson. Med.* **52**, 100–107 (2004).
87. Kamimura, H. A. et al. Feedback control of microbubble cavitation for ultrasound-mediated blood-brain barrier disruption in non-human primates under magnetic resonance guidance. *J. Cereb. Blood Flow. Metab.* **39**, 1191–1203 (2019).
88. Lipsman, N. et al. Blood-brain barrier opening in Alzheimer's disease using MR-guided focused ultrasound. *Nat. Commun.* **9**, 2336 (2018).
89. Muthupillai, R. et al. Magnetic resonance elastography by direct visualization of propagating acoustic strain waves. *Science* **269**, 1854–1857 (1995).
90. Plewes, D. B., Betty, I., Urchuk, S. N. & Soutar, I. Visualizing tissue compliance with MR imaging. *J. Magn. Reson Imaging* **5**, 733–738 (1995).
91. Larrat, B. et al. MR-guided transcranial brain HIFU in small animal models. *Phys. Med. Biol.* **55**, 365–388 (2010).
92. Kaye, E. A. & Pauly, K. B. Adapting MRI acoustic radiation force imaging for in vivo human brain focused ultrasound applications. *Magn. Reson. Med.* **69**, 724–733 (2013).
93. Wu, C. H. et al. Monitoring of acoustic cavitation in microbubble-presented focused ultrasound exposure using gradient-echo MRI. *J. Magn. Reson Imaging* **51**, 311–318 (2020).
94. Huang, Y., Alkins, R., Schwartz, M. L. & Hynynen, K. Opening the blood-brain barrier with MR Imaging-guided focused ultrasound: preclinical testing on a trans-human skull Porcine model. *Radiology* **282**, 123–130 (2017).
95. Carpentier, A. et al. Clinical trial of blood-brain barrier disruption by pulsed ultrasound. *Sci. Transl. Med.* **8**, 343re342 (2016).
96. Lynn, J. G., Zwemer, R. L., Chick, A. J. & Miller, A. E. A new method for the generation and use of focused ultrasound in experimental biology. *J. Gen. Physiol.* **26**, 179–193 (1942).
97. Ishihara, Y. et al. A precise and fast temperature mapping using water proton chemical shift. *Magn. Reson. Med.* **34**, 814–823 (1995).
98. Choquet, K. et al. Magnetic Resonance Acoustic Radiation Force Imaging (MR-ARFI) for the monitoring of High Intensity Focused Ultrasound (HIFU) ablation in anisotropic tissue. *Magma* **36**, 737–747 (2023).
99. Arvanitis, C. D., Livingstone, M. S. & McDannold, N. Combined ultrasound and MR imaging to guide focused ultrasound therapies in the brain. *Phys. Med Biol.* **58**, 4749–4761 (2013).
100. Haworth, K. J. et al. Passive imaging with pulsed ultrasound insonations. *J. Acoust. Soc. Am.* **132**, 544–553 (2012).
101. Burgess, M. T., Apostolakis, I. & Konofagou, E. E. Power cavitation-guided blood-brain barrier opening with focused ultrasound and microbubbles. *Phys. Med. Biol.* **63**, 065009 (2018).
102. Song, K. H., Harvey, B. K. & Borden, M. A. State-of-the-art of microbubble-assisted blood-brain barrier disruption. *Theranostics* **8**, 4393–4408 (2018).
103. Lv, J., Roy, S., Xie, M., Yang, X. & Guo, B. Contrast Agents of Magnetic Resonance Imaging and Future Perspective. *Nanomaterials***13**, 2003 (2023).
104. O'Reilly, M. A., Waspe, A. C., Ganguly, M. & Hynynen, K. Focused-ultrasound disruption of the blood-brain barrier using closely-timed short pulses: influence of sonication parameters and injection rate. *Ultrasound Med. Biol.* **37**, 587–594 (2011).
105. Chavhan, G. B., Babyn, P. S., Thomas, B., Shroff, M. M. & Haacke, E. M. Principles, techniques, and applications of T2*-based MR imaging and its special applications. *Radiographics* **29**, 1433–1449 (2009).
106. Haacke, E. M., Mittal, S., Wu, Z., Neelavalli, J. & Cheng, Y. C. Susceptibility-weighted imaging: technical aspects and clinical applications, part 1. *AJNR Am. J. Neuroradiol.* **30**, 19–30 (2009).
107. Liu, H. L. et al. Magnetic resonance imaging enhanced by superparamagnetic iron oxide particles: usefulness for distinguishing between focused ultrasound-induced blood-brain barrier disruption and brain hemorrhage. *J. Magn. Reson Imaging* **29**, 31–38 (2009).
108. Sinharay, S. et al. In vivo imaging of sterile microglial activation in rat brain after disrupting the blood-brain barrier with pulsed focused ultrasound: [18F]DPA-714 PET study. *J. Neuroinflamm.***16**, 155 (2019).
109. Tu, T. W. et al. Diffusion tensor imaging and chemical exchange saturation transfer MRI evaluation on the long-term effects of pulsed focused ultrasound and microbubbles blood brain barrier opening in the rat. *Front Neurosci.* **14**, 908 (2020).
110. Blackmore, J., Shrivastava, S., Sallet, J., Butler, C. R. & Cleveland, R. O. Ultrasound neuromodulation: a review of results, mechanisms and safety. *Ultrasound Med Biol.* **45**, 1509–1536 (2019).
111. Deffieux, T. et al. Low-intensity focused ultrasound modulates monkey visuomotor behavior. *Curr. Biol.* **23**, 2430–2433 (2013).
112. Ogawa, S., Lee, T. M., Kay, A. R. & Tank, D. W. Brain magnetic resonance imaging with contrast dependent on blood oxygenation. *Proc. Natl. Acad. Sci. USA* **87**, 9868–9872 (1990).
113. Todd, N. et al. Modulation of brain function by targeted delivery of GABA through the disrupted blood-brain barrier. *Neuroimage* **189**, 267–275 (2019).
114. Liu, D. et al. Alteration of functional connectivity in the cortex and major brain networks of non-human primates following focused

ultrasound exposure in the dorsal striatum. *Brain Stimul.* **16**, 1196–1204 (2023).
115. Jung, O. et al. Neuroinflammation associated with ultrasound-mediated permeabilization of the blood-brain barrier. *Trends Neurosci.* **45**, 459–470 (2022).
116. Kreisl, W. C. et al. PET imaging of neuroinflammation in neurological disorders. *Lancet Neurol.* **19**, 940–950 (2020).
117. Hammoud, D. A. Molecular imaging of inflammation: current status. *J. Nucl. Med* **57**, 1161–1165 (2016).
118. Chen, K. T. et al. Neuronavigation-guided focused ultrasound for transcranial blood-brain barrier opening and immunostimulation in brain tumors. *Sci. Adv.* **7**, eabd0772 (2021).
119. D'Haese, P. F. et al. β-amyloid plaque reduction in the hippocampus after focused ultrasound-induced blood-brain barrier opening in Alzheimer's disease. *Front Hum. Neurosci.* **14**, 593672 (2020).
120. Meng, Y. et al. MR-guided focused ultrasound liquid biopsy enriches circulating biomarkers in patients with brain tumors. *Neuro Oncol.* **23**, 1789–1797 (2021).
121. Sonabend, A. M. et al. Repeated blood-brain barrier opening with an implantable ultrasound device for delivery of albumin-bound paclitaxel in patients with recurrent glioblastoma: a phase 1 trial. *Lancet Oncol.* **24**, 509–522 (2023).
122. Abrahao, A. et al. First-in-human trial of blood-brain barrier opening in amyotrophic lateral sclerosis using MR-guided focused ultrasound. *Nat. Commun.* **10**, 4373 (2019).
123. Gasca-Salas, C. et al. Blood-brain barrier opening with focused ultrasound in Parkinson's disease dementia. *Nat. Commun.* **12**, 779 (2021).
124. Bae, S. et al. Transcranial blood-brain barrier opening in Alzheimer's disease patients using a portable focused ultrasound system with real-time 2-D cavitation mapping. *Theranostics* **14**, 4519–4535 (2024).
125. Jung, B. A. & Weigel, M. Spin echo magnetic resonance imaging. *J. Magn. Reson Imaging* **37**, 805–817 (2013).
126. Park, S. H. et al. Safety and feasibility of multiple blood-brain barrier disruptions for the treatment of glioblastoma in patients undergoing standard adjuvant chemotherapy. *J. Neurosurg.* **134**, 475–483 (2020).
127. Idbaih, A. et al. Safety and feasibility of repeated and transient blood-brain barrier disruption by pulsed ultrasound in patients with recurrent Glioblastoma. *Clin. Cancer Res. : Off. J. Am. Assoc. Cancer Res.* **25**, 3793–3801 (2019).
128. Mehta, R. I. et al. Blood-brain barrier opening with MRI-guided focused ultrasound elicits meningeal venous permeability in humans with early Alzheimer disease. *Radiology* **298**, 654–662 (2021).
129. Pineda-Pardo, J. A. et al. Striatal blood-brain barrier opening in Parkinson's disease dementia: a pilot exploratory study. *Mov. Disord.* **37**, 2057–2065 (2022).
130. Chang, K. W., Hong, S. W., Chang, W. S., Jung, H. H. & Chang, J. W. Characteristics of Focused Ultrasound Mediated Blood-Brain Barrier Opening in Magnetic Resonance Images. *J. Korean Neurosurg. Soc.* **66**, 172–182 (2023).
131. Mainprize, T. et al. Blood-brain barrier opening in primary brain tumors with non-invasive MR-guided focused ultrasound: a clinical safety and feasibility study. *Sci. Rep.* **9**, 321 (2019).
132. Huang, Y. et al. Cavitation feedback control of focused ultrasound blood-brain barrier opening for drug delivery in patients with Parkinson's disease. *Pharmaceutics* **14**, 2607 (2022).
133. Rezai, A. R. et al. Focused ultrasound-mediated blood-brain barrier opening in Alzheimer's disease: long-term safety, imaging, and cognitive outcomes. *J. Neurosurg.* **139**, 275–283 (2023).
134. Mehta, R. I. et al. Ultrasound-mediated blood-brain barrier opening uncovers an intracerebral perivenous fluid network in persons with Alzheimer's disease. *Fluids Barriers CNS* **20**, 46 (2023).
135. Rezai, A. R. et al. Ultrasound blood-brain barrier opening and Aducanumab in Alzheimer's disease. *N. Engl. J. Med* **390**, 55–62 (2024).
136. Jeong, H. et al. A pilot clinical study of low-intensity transcranial focused ultrasound in Alzheimer's disease. *Ultrasonography* **40**, 512–519 (2021).
137. Gasca-Salas, C. et al. Nigrostriatal blood-brain barrier opening in Parkinson's disease. *J Neurol. Neurosurg. Psychiatry*, **95**, 1089–1092 (2024).
138. Meng, Y. et al. Putaminal Recombinant Glucocerebrosidase delivery with magnetic resonance-guided focused ultrasound in Parkinson's disease: a Phase I study. *Mov. Disord.* **37**, 2134–2139 (2022).
139. Park, S. H. et al. Extensive frontal focused ultrasound mediated blood-brain barrier opening for the treatment of Alzheimer's disease: a proof-of-concept study. *Transl. Neurodegener.* **10**, 44 (2021).
140. Epelbaum, S. et al. Pilot study of repeated blood-brain barrier disruption in patients with mild Alzheimer's disease with an implantable ultrasound device. *Alzheimers Res. Ther.* **14**, 40 (2022).
141. Carpentier, A. et al. Repeated blood-brain barrier opening with a nine-emitter implantable ultrasound device in combination with carboplatin in recurrent glioblastoma: a phase I/II clinical trial. *Nat. Commun.* **15**, 1650 (2024).
142. Anastasiadis, P. et al. Localized blood-brain barrier opening in infiltrating gliomas with MRI-guided acoustic emissions-controlled focused ultrasound. *Proc. Natl. Acad. Sci. USA* **118**, e2103280118 (2021).
143. Meng, Y. et al. MR-guided focused ultrasound enhances delivery of trastuzumab to Her2-positive brain metastases. *Sci. Transl. Med.* **13**, eabj4011 (2021).
144. Burgess, A. et al. Alzheimer disease in a mouse model: MR imaging-guided focused ultrasound targeted to the hippocampus opens the blood-brain barrier and improves pathologic abnormalities and behavior. *Radiology* **273**, 736–745 (2014).
145. Leinenga, G. & Götz, J. Scanning ultrasound removes amyloid-β and restores memory in an Alzheimer's disease mouse model. *Sci. Transl. Med.* **7**, 278ra233 (2015).
146. McMahon, D., Bendayan, R. & Hynynen, K. Acute effects of focused ultrasound-induced increases in blood-brain barrier permeability on rat microvascular transcriptome. *Sci. Rep.* **7**, 45657 (2017).
147. Pekny, M., Wilhelmsson, U. & Pekna, M. The dual role of astrocyte activation and reactive gliosis. *Neurosci. Lett.* **565**, 30–38 (2014).
148. Tamrazi, B. et al. Changes in signal intensity of the Dentate Nucleus and Globus Pallidus in pediatric patients: impact of brain irradiation and presence of primary brain tumors independent of linear Gadolinium-based contrast agent administration. *Radiology* **287**, 452–460 (2018).
149. Cao, Y. et al. Effect of renal function on Gadolinium-related signal increases on unenhanced T1-weighted brain magnetic resonance imaging. *Invest. Radio.* **51**, 677–682 (2016).
150. Malheiros, J. M., Paiva, F. F., Longo, B. M., Hamani, C. & Covolan, L. Manganese-enhanced MRI: Biological applications in neuroscience. *Front. Neurol.* **6**, 161 (2015).
151. Petcharunpaisan, S., Ramalho, J. & Castillo, M. Arterial spin labeling in neuroimaging. *World J. Radio.* **2**, 384–398 (2010).
152. Caballero-Insaurriaga, J. et al. Zero TE MRI applications to transcranial MR-guided focused ultrasound: Patient screening and treatment efficiency estimation. *J. Magn. Reson Imaging* **50**, 1583–1592 (2019).
153. Guo, S. et al. Feasibility of ultrashort echo time images using full-wave acoustic and thermal modeling for transcranial MRI-guided focused ultrasound (tcMRgFUS) planning. *Phys. Med. Biol.* **64**, 095008 (2019).
154. Manuel T. J. et al. Ultra-short time-echo based ray tracing for transcranial focused ultrasound aberration correction in human

calvaria. *Phys. Med. Biol*. **70**, https://doi.org/10.1088/1361-6560/ad4f44 (2025).
155. Englander, Z. K. et al. Focused ultrasound mediated blood-brain barrier opening is safe and feasible in a murine pontine glioma model. *Sci. Rep.* **11**, 6521 (2021).
156. Hynynen, K., McDannold, N., Sheikov, N. A., Jolesz, F. A. & Vykhodtseva, N. Local and reversible blood-brain barrier disruption by noninvasive focused ultrasound at frequencies suitable for trans-skull sonications. *Neuroimage* **24**, 12–20 (2005).
157. O'Reilly, M. A. & Hynynen, K. Blood-brain barrier: real-time feedback-controlled focused ultrasound disruption by using an acoustic emissions-based controller. *Radiology* **263**, 96–106 (2012).
158. Huang, Q. et al. Targeted gene delivery to the mouse brain by MRI-guided focused ultrasound-induced blood-brain barrier disruption. *Exp. Neurol.* **233**, 350–356 (2012).
159. Yang, F. Y., Liu, S. H., Ho, F. M. & Chang, C. H. Effect of ultrasound contrast agent dose on the duration of focused-ultrasound-induced blood-brain barrier disruption. *J. Acoust. Soc. Am.* **126**, 3344–3349 (2009).
160. Yang, F. Y., Horng, S. C., Lin, Y. S. & Kao, Y. H. Association between contrast-enhanced MR images and blood-brain barrier disruption following transcranial focused ultrasound. *J. Magn. Reson Imaging* **32**, 593–599 (2010).
161. Jones, R. M. et al. Three-dimensional transcranial microbubble imaging for guiding volumetric ultrasound-mediated blood-brain barrier opening. *Theranostics* **8**, 2909–2926 (2018).
162. Kobus, T., Vykhodtseva, N., Pilatou, M., Zhang, Y. & McDannold, N. Safety validation of repeated blood-brain barrier disruption using focused ultrasound. *Ultrasound Med. Biol.* **42**, 481–492 (2016).
163. Marquet, F. et al. Real-time, transcranial monitoring of safe blood-brain barrier opening in non-human primates. *PLoS One* **9**, e84310 (2014).
164. Chien, C. Y., Xu, L., Pacia, C. P., Yue, Y. & Chen, H. Blood-brain barrier opening in a large animal model using closed-loop microbubble cavitation-based feedback control of focused ultrasound sonication. *Sci. Rep.* **12**, 16147 (2022).
165. Fadera, S. et al. Focused ultrasound-mediated delivery of anti-programmed cell death-Ligand 1 antibody to the brain of a Porcine Model. *Pharmaceutics* **15**, 2479 (2023).
166. O'Reilly, M. A. et al. Investigation of the safety of focused ultrasound-induced blood-brain barrier opening in a natural canine model of aging. *Theranostics* **7**, 3573–3584 (2017).
167. Hu, Z., Chen, S., Yang, Y., Gong, Y. & Chen, H. An affordable and easy-to-use focused ultrasound device for noninvasive and high precision drug delivery to the mouse brain. *IEEE Trans. Biomed. Eng.* **69**, 2723–2732 (2022).
168. Schregel, K. et al. Targeted blood brain barrier opening with focused ultrasound induces focal macrophage/microglial activation in experimental autoimmune encephalomyelitis. *Front. Neurosci.* **15**, 665722 (2021).
169. Todd, N. et al. Focused ultrasound induced opening of the blood-brain barrier disrupts inter-hemispheric resting state functional connectivity in the rat brain. *Neuroimage* **178**, 414–422 (2018).
170. Xia, J., Tsui, P. H. & Liu, H. L. Low-pressure burst-mode focused ultrasound wave reconstruction and mapping for blood-brain barrier opening: a preclinical examination. *Sci. Rep.* **6**, 27939 (2016).
171. Novell, A. et al. A new safety index based on intrapulse monitoring of ultra-harmonic cavitation during ultrasound-induced blood-brain barrier opening procedures. *Sci. Rep.* **10**, 10088 (2020).
172. Le Floc'h, J. et al. Transcranial photoacoustic detection of blood-brain barrier disruption following focused ultrasound-mediated nanoparticle delivery. *Mol. Imaging Biol.* **22**, 324–334 (2020).
173. Lapin, N. A., Gill, K., Shah, B. R. & Chopra, R. Consistent opening of the blood brain barrier using focused ultrasound with constant intravenous infusion of microbubble agent. *Sci. Rep.* **10**, 16546 (2020).
174. Curley, C. T. et al. Augmentation of brain tumor interstitial flow via focused ultrasound promotes brain-penetrating nanoparticle dispersion and transfection. *Sci. Adv.* **6**, eaay1344 (2020).
175. Alli, S. et al. Brainstem blood brain barrier disruption using focused ultrasound: A demonstration of feasibility and enhanced doxorubicin delivery. *J. Control Release* **281**, 29–41 (2018).
176. Lin, C. Y. et al. Non-invasive, neuron-specific gene therapy by focused ultrasound-induced blood-brain barrier opening in Parkinson's disease mouse model. *J. Control Release* **235**, 72–81 (2016).
177. Chu, P. C. et al. Pharmacodynamic analysis of magnetic resonance imaging-monitored focused ultrasound-induced blood-brain barrier opening for drug delivery to brain tumors. *BioMed. Res. Int.* **2013**, 627496 (2013).
178. Rich, M. C. et al. Focused ultrasound blood brain barrier opening mediated delivery of MRI-visible albumin nanoclusters to the rat brain for localized drug delivery with temporal control. *J. Control Release* **324**, 172–180 (2020).
179. Olumolade, O. O., Wang, S., Samiotaki, G. & Konofagou, E. E. Longitudinal motor and behavioral assessment of blood-brain barrier opening with transcranial focused ultrasound. *Ultrasound Med Biol.* **42**, 2270–2282 (2016).
180. Grudzenski, S. et al. Simulation, implementation and measurement of defined sound fields for blood-brain barrier opening in rats. *Ultrasound Med Biol.* **48**, 422–436 (2022).
181. Martinez, P. et al. MRI-guided focused ultrasound blood-brain barrier opening increases drug delivery and efficacy in a diffuse midline glioma mouse model. *Neurooncol. Adv.* **5**, vdad111 (2023).
182. Wei, H. J. et al. Focused ultrasound-mediated blood-brain barrier opening increases delivery and efficacy of etoposide for glioblastoma treatment. *Int J. Radiat. Oncol. Biol. Phys.* **110**, 539–550 (2021).
183. Tazhibi, M. et al. Focused ultrasound-mediated blood-brain barrier opening is safe and feasible with moderately hypofractionated radiotherapy for brainstem diffuse midline glioma. *J. Transl. Med.* **22**, 320 (2024).
184. Xu, L., Gong, Y., Chien, C. Y., Leuthardt, E. & Chen, H. Transcranial focused ultrasound-induced blood–brain barrier opening in mice without shaving hairs. *Sci. Rep.* **13**, 13500 (2023).
185. Galan-Acosta, L. et al. Recombinant BRICHOS chaperone domains delivered to mouse brain parenchyma by focused ultrasound and microbubbles are internalized by hippocampal and cortical neurons. *Mol. Cell Neurosci.* **105**, 103498 (2020).
186. Fan, C. H. et al. Contrast-enhanced ultrasound imaging for the detection of focused ultrasound-induced blood-brain barrier opening. *Theranostics* **4**, 1014–1025 (2014).
187. Chu, P. C. et al. Focused ultrasound-induced blood-brain barrier opening: association with mechanical index and cavitation index analyzed by dynamic contrast-enhanced magnetic-resonance imaging. *Sci. Rep.* **6**, 33264 (2016).
188. Chai, W. Y. et al. Image-guided focused-ultrasound CNS molecular delivery: an implementation via dynamic contrast-enhanced magnetic-resonance imaging. *Sci. Rep.* **8**, 4151 (2018).
189. Choi, H. J. et al. The new insight into the inflammatory response following focused ultrasound-mediated blood-brain barrier disruption. *Fluids Barriers CNS* **19**, 103 (2022).
190. Wang, S. et al. Focused ultrasound induced-blood-brain barrier opening in mouse brain receiving radiosurgery dose of radiation enhances local delivery of systemic therapy. *Br. J. Radio.* **93**, 20190214 (2020).
191. Vlachos, F., Tung, Y. S. & Konofagou, E. E. Permeability assessment of the focused ultrasound-induced blood-brain barrier opening

using dynamic contrast-enhanced MRI. *Phys. Med. Biol.* **55**, 5451–5466 (2010).
192. Huh, H. et al. A local difference in blood-brain barrier permeability in the caudate putamen and thalamus of a rat brain induced by focused ultrasound. *Sci. Rep.* **10**, 19286 (2020).
193. Rezai, A. R. et al. Noninvasive hippocampal blood-brain barrier opening in Alzheimer's disease with focused ultrasound. *Proc. Natl. Acad. Sci. USA* **117**, 9180–9182 (2020).

Acknowledgements

The authors acknowledge the Agence Nationale pour la Recherche for financial support (ANR-24-CE19-5885).

Author contributions

G.P. wrote the initial draft and prepared the figures. A.N. and B.L. discussed, read, reviewed, edited, and approved the manuscript.

Competing interests

B.L. and A.N. are stockholders of a company developing an ultrasound device for blood-brain barrier opening. G.P. declares no competing interests.

Additional information

Correspondence and requests for materials should be addressed to Anthony Novell.